SSSU 89
ISSN 0140 3818

EXPERIMENTAL MEASUREMENTS OF THE SEAKEEPING CHARACTERISTICS OF FAST DISPLACEMENT CATAMARANS IN LONG-CRESTED HEAD-SEAS

J.F. Wellicome, P. Temarel, A.F. Molland and P.R. Couser

Ship Science Report 89

December 1995

SSSU 89
ISSN 0140 3818

UNIVERSITY OF SOUTHAMPTON

DEPARTMENT OF SHIP SCIENCE

FACULTY OF ENGINEERING AND APPLIED SCIENCE

EXPERIMENTAL MEASUREMENTS OF THE SEAKEEPING CHARACTERISTICS OF FAST DISPLACEMENT CATAMARANS IN LONG-CRESTED HEAD-SEAS

J.F. Wellicome, P. Temarel, A.F. Molland and P.R. Couser

Ship Science Report 89

December 1995

Ship Science Report No. 89
Experimental Measurements of the Seakeeping Characteristics of Fast Displacement Catamarans in Long-Crested Head-Seas

Dr J.F. Wellicome, Dr P. Temarel, Dr A.F. Molland and Mr P.R. Couser

December 1995

Abstract

The report describes an experimental investigation into the seakeeping properties of catamarans. Three geometrically similar hull forms were tested covering a range of Length:Displacement ratio from 7.4 to 9.5. The hulls are of round bilge transom stern form and are based on the NPL round bilge series. A number of hull configurations, including monohull and two catamaran demihull spacings, were tested at three Froude numbers (F_n = 0.2, 0.53, 0.8) and over a range of wavelengths. Long-crested head-seas were used for all experiments. Measurements of heave, pitch, vertical acceleration at two stations and added resistance in waves were made. Response functions have been calculated from both regular and irregular wave experiments.

Contents

Nomenclature

Symbols and some values used in the report:

Demihull	One of the hulls which make up the catamaran
LCG	Longitudinal centre of gravity
TF	Transfer function
RMS	Route mean square
FFT	Fast Fourier transform
F_n	Froude Number, $[u/\sqrt{gL}]$
R_e	Reynolds Number, $[uL/\nu]$
u	Velocity [ms^{-1}]
L, L_{BP}	Demihull length between perpendiculars [m]
A, WSA	Static wetted surface area [m^2]
B	Demihull maximum beam [m]
T	Demihull draught [m]
S	Separation between catamaran (demihull) centrelines [m]
∇	Volume of displacement (demihull)[m^3]
Δ	Mass displacement in freshwater (demihull)[kg]
C_B	Block coefficient (demihull)
C_P	Prismatic coefficient (demihull)
C_M	Midship section area coefficient (demihull)
$L/\nabla^{\frac{1}{3}}$	Length : displacement ratio (demihull)
γ	Ship : Model scale factor
Added res. coeff.	$\Delta R/(2\zeta^2_{\mathrm{RMS}}\rho g B^2/L)$ or $\Delta R/(\zeta^2\rho g B^2/L)$
λ	Wavelength [m]
ζ	Wave amplitude [m]
$h_{\frac{1}{3}}$	Significant wave height
T_0	Wave period, spectrum characteristic period [s]
ω, ω_0	Wave circular frequency [$rads^{-1}$]
ω_e	Wave encounter circular frequency [$rads^{-1}$]
μ	Ship heading [rad] (0=following seas, π=head seas)
$TF(\omega_e)$	Transfer function spectrum
$E_w(\omega_e)$	Wave energy spectrum
$M(\omega_e)$	Motion spectrum
m_0	Zero moment of spectrum (area under spectrun)
g	Acceleration due to gravity [9.80665 ms^{-2}]
ρ	Density of freshwater [1000 kg/ m^3]
ν	Kinematic viscosity of freshwater [1.141×10^{-6} m^2s^{-1} at 15°C]

1 Introduction

The design of conventional ships has tended to concentrate on calm water performance. However, as operating speeds increase the rough water seakeeping characteristics become more important. The vessels under investigation in this report operate up to a Froude number of unity which corresponds to speeds of 19, 27 and 39 kts for ships of lengths 10, 20 and 40m respectively. At these speeds operation in even relatively low sea states becomes important and the seakeeping performance should be determined early in the design process.

Seakeeping design criteria vary depending on the rôle of the vessel but generally can be reduced to permissible limits of root mean square (RMS) accelerations and motions. A vessel's performance should, ideally, not be limited by a single criterion; all the limiting criteria should occur under approximately the same conditions. Hence, a detailed understanding of vessel response, operating sea conditions and limiting criteria are required.

Calm water resistance characteristics of catamarans have been examined in detail at the University of Southampton over a number of years (Insel, 1990; Insel and Molland, 1992; Molland et al., 1994). Attention has now been directed towards their seakeeping performance. The characteristics of a range of catamaran configurations in long-crested head-seas have been investigated at the University of Southampton, and the results of the work are contained in this report.

2 Details of models

A total of three hullforms have been tested. The models are a subset of those used in the investigation into catamaran calm water resistance (Molland et al., 1994); the same model notation has been used for this investigation. Details of the models are given in Table1.

The models were of symmetrical round bilge form with transom sterns, see Figure 1, and were derived from the NPL round bilge series(Marwood and Bailey, 1969; Bailey, 1976). This broadly represents the underwater form of a number of catamarans in service or currently under construction. The models were tested in both monohull and catamaran configurations.

The models were manufactured using moulds taken from the foam hulls used in the calm water experiments (Molland et al., 1994). An epoxy-foam sandwich skin was used and this gave excellent strength to weight ratios for the models. The length of model 6b was increased from 1.6m to 2.1m in order to achieve a satisfactory weight-displacement balance. The models were fitted with turbulence stimulation comprising trip studs of 3.2mm diameter and 2.5mm height at a spacing of 25mm. The studs were situated 37.5mm aft of the stem. The models were tested without underwater appendages.

The towing point was set coincident with the longitudinal (LCG) and vertical centres of gravity (VCG) where the VCG was 1.5 Draught above the base line. The longitudinal moment of inertia in pitch was set such that the longitudinal radius of gyration was 25% of the length of the model. It should be noted that the moving mass in pitch was less than that in heave. This was because the tow post and part of the tow fitting moved only in heave and were not free to pitch. Depending on the particular model the towpost represented 8.2%, 12.4% and 7.6% of the catamaran displacement of models 4b, 5b and 6b[1] respectively.

No compensation was made for the vertical separation of the tow point and the propeller thrust line. The tow fitting allowed free movement in heave and pitch whilst movements in surge, sway, roll and yaw were restrained.

3 Facilities and Tests

3.1 Tank Facilities

The model experiments were carried out in the Southampton Institute test tank. The principal particulars of the tank are given in Table 2.

For most conditions the steady speed run length was 15.24m. This was extended to approximately 25m for the slowest model speed where less acceleration distance was required.

The tank is fitted with a paddle-type wave maker at one end and a passive beach at the opposite end. The wave maker is computer controlled and is capable of generating both regular and irregular waves. Irregular waves are defined by a power spectrum such as ITTC, Jonswap or Pierson Moskowitz. Waves can be generated at various frequencies and wave heights dependent on the response of the wavemakers and the size and type of model being tested. The frequency range is from about 2.5Hz to 0.6Hz. The

[1] Despite having the largest $L/\nabla^{\frac{1}{3}}$ Model 6b had the greatest displacement due to its increased length.

lowest frequency is determined by the longest wave possible in the tank without being affected by the tank bottom; this corresponds to a wave length of approximately 4.5m.

3.2 Instrumentation

Heave motions were measured with a linear potentiometer mounted at the longitudinal centre of gravity. Pitch was measured with an angular potentiometer in the tow fitting. Accelerations were measured using piezoresistive accelerometers at the longitudinal centre of gravity and 15% of the length of the model aft of the forward perpendicular. The wave system encountered during the run was measured with a stiff, sword type, resistance wave probe mounted on the carriage ahead and to the side of the model. Comparisons of traces recorded from the carriage using this probe and from a shore based probe showed satisfactory correlation. All signals were acquired using a microcomputer via an analogue to digital converter. This system enabled detailed analysis of the results from each run to be carried out during the experiments. The wave maker was found to produce waves of the requested period but wave amplitudes showed some variation with frequency.

3.3 Test Conditions

Only head sea tests have been carried out; following Lloyd (1989, p326), the maximum model length for following sea tests is one quarter of the tank breadth, this limitation would result in models which would be too small to produce useful results. Test were carried out in three hull configurations: monohull, and in catamaran mode with Separation:Length ratios (S/L) of 0.2 and 0.4. Measurements of each model configuration were taken at three Froude numbers (F_n = 0.20, 0.53 and 0.80) and over an encounter frequency range of 6 rads^{-1} to 16 rads^{-1} . An exception was for Model 4b at the closest spacing $S/L = 0.2$ where the bow waves between the demihulls was too large to allow the highest Froude number case. The relationship between encounter frequency and ship-length to wavelength ratio L/λ for the three speeds is given in Table 3.

4 Data Reduction and Corrections

During regular wave tests the models were allowed to encounter at least five to six waves before the responses were recorded, so as to allow transients in the response to die out. The models then encountered a minimum of six waves during which the measurements were taken. At the higher encounter frequencies many more waves were encountered.

Regular wave tests were analysed using two methods. Firstly, RMS values of the measured motions and the programmed wave frequency were used to calculated the transfer functions. Secondly, a least-squares sine wave fit was made to the measured motions — see Appendix A for details. This enabled the amplitude, period, and most importantly the phase relationships to be accurately determined. Good correlation between the two methods was found. The accuracy of the accelerometer measurements was also confirmed by twice differentiating the vertical motions at the accelerometer positions. These derived accelerations were found to match, very closely, the directly measured values.

Transfer functions from the regular wave experiments were calculated as follows:

$$\text{Heave TF} = \frac{\text{Heave Amplitude RMS}}{\text{Wave Amplitude RMS}}$$

$$\text{Pitch TF} = \frac{\text{Pitch Amplitude RMS[rad]}}{\text{Wave Amplitude RMS[m]}} \times \frac{g[\ \text{ms}^{-2}\ ]}{\omega_0^2[\ \text{rads}^{-1}\ ]} \tag{1}$$

$$\text{Accel TF} = \frac{\text{Accel Amplitude RMS}[\ \text{ms}^{-2}\ ]}{\text{Wave Amplitude RMS[m]}} \times \frac{1}{\omega_e^2[\ \text{rads}^{-1}\ ]}$$

where the encounter frequency ω_e is related to the wave frequency ω_0 by Equation 2; u is the ship speed and μ the ship heading with $\mu = 0$ for the following sea case and $\mu = \pi$ for the head sea case.

$$\omega_e = \omega_0 - \cos(\mu)\frac{\omega_0^2 u}{g} \tag{2}$$

Data from random wave experiments were also used to calculate the motion transfer functions. The time domain measurements were transformed into the frequency domain using a fast fourier transform (FFT) method. The transfer functions were calculated from the response spectra using Equations 1

described above, noting that the square root of the spectral data must be used in calculating the transfer functions. Due to the short run time and hence limited time series data available, especially during high speed tests, problems were encountered in obtaining reliable response and wave spectra by the FFT method. Several methods were tried including maximum likelihood and maximum entropy methods as well as several windowing techniques for the FFT. The method finally adopted for the results presented here was a FFT using a Hanning window on the data, details of which are given in Appendix C. Software developed by the Wolfson Unit MTIA was used to analyse the data from the experiments. To obtain reliable spectral estimates the spectra of a number of runs with slightly varying characteristic period and significant wave height were averaged. Using this method good correlation between the transfer functions obtained from regular and irregular wave tests was found.

Added resistance was calculated from the regular wave data (note: the model was kept fixed in surge). The dynamometer was sufficiently stiff for the rise and fall in resistance during each wave cycle to be clearly visible on the resistance measurement trace. Added resistance was assumed to be proportional to wave height squared (this was confirmed at several test conditions by varying the wave amplitude) and has been presented in terms of an added resistance coefficient given in Equation 3. Note that the factor of 2 is included since, for a sine wave signal, the RMS is $1/\sqrt{2}$ of the signal amplitude.

$$\text{Added Res. Coeff.} = \frac{R_{\text{reg. waves}} - R_{\text{calm water}}}{2\zeta_{\text{RMS}}^2 \rho g B^2 / L} \tag{3}$$

The tank temperature was monitored but not found to vary significantly. Tank blockage effects were investigated in detail by Insel (1990) and Molland et al. (1994) and found to be small. For these reasons no corrections were applied to the data.

5 Discussion of Results

5.1 Motions

5.1.1 Experimental Results

The basic experimental data are presented on the following pages. Motions transfer functions have been calculated from both regular and irregular wave tests, whilst the phase relationships between the various motions and the encountered wave system have been calculated from the regular tests only. The transfer functions have been calculated according to Equation 1. The phase figures show the phase angle between the wave at the centre of gravity of the hull and the response of interest. (The phase presented for the forward acceleration is the phase difference between the acceleration measurement and wave at the centre of gravity.) The graphs are plotted with circular wave encounter frequency as abscissa; Table 4 shows how these may be converted to wavelength:ship-length ratios for the different speeds tested.

The results for the monohull (Figures 2 to 10) are as expected and follow the classical transfer function shapes. It should be noted that the acceleration at LCG shows excellent correlation with the heave response in both magnitude and phase (this was found to be true for all the tests). A similar correlation was found between the measured forward acceleration and that calculated form the second derivative of the vertical motion at that point. The amplitude of the vertical motion was calculated from the amplitudes and phases of the heave and pitch transfer functions. The agreement between the transfer functions calculated from regular and irregular waves is excellent at the slower speeds but not so good at the higher speeds. This can be attributed to several phenomena.

- At the higher speeds the run time is greatly shortened reducing the number of points in the frequency range of interest after the FFT has been used to calculate the response spectra.
- The wave trace is measured in front of the model centre of gravity (to avoid interference). This results in the measured irregular waves not corresponding exactly to the waves that generated the measured model motions. This is because the recorded wave trace effectively starts and ends slightly after those of the recorded motions. In the case of regular waves this can be accounted for by a phase shift.
- These results indicate that non-linear effects may be greater at higher speeds which is what might be expected.

The results for the catamarans are given in Figures 11 to 25. In most cases these show similar trends to the monohull results except at the lowest speed ($F_n = 0.2$) where a secondary peak in the heave response can be noted. At the higher speeds there appears to be some spreading of the peak.

Figures 80 to 85 show the effect of speed on the responses for the various hull configurations. These results are as expected with the transfer functions increasing with increase in forward speed. It is interesting to note that for pitch this phenomenon is not so well defined and some overlap in the $F_n = 0.5$ and $F_n = 0.8$ results can be found. This is also reflected in the forward acceleration transfer function where pitch plays an important part.

Figures 86 to 91 show the effect of hull spacing on the transfer functions at the different speeds tested. There is little significant difference between the responses except at the lowest speed, and here only in heave (and hence LCG acceleration). This is because it is only at these lower speeds that the waves generated from one hull impinge on the other; at higher speed they pass behind the other demihull. The effect is most pronounced at $S/L = 0.2$ and occurs at an encounter frequency of 11.5 rads^{-1} . At the higher spacing there are two smaller peaks. This is likely to be due to the increased number of oscillating wave modes possible between the demihulls at this spacing.

5.1.2 Comparison of RMS responses

Although a detailed analysis of the transfer functions can provide an excellent insight into the effect of hull spacing and other design parameters, the actual responses of the vessels in appropriate sea states should be used to determine the best design. The RMS motions and accelerations, based on the results for Model 4b, have been calculated for three wave spectra using the ITTC two parameter spectrum. A summary of the method used is given in Appendix D. The spectra cover a range of characteristic periods but significant wave height has been fixed at 2.0m to aid comparison. (It should be noted that the RMS responses are directly proportional to wave height; hence the responses for higher sea states may easily be calculated. However in general there is a reasonably correlated relationship between significant wave height and characteristic period which depends on the sea area of intereast and the prevailing direction

the wave system.) A summary of the spectra is given in Table 5. These spectra broadly cover the range of characteristic periods found on likely catamaran routes. (Table 6 shows the characteristic periods and significant wave heights for various sea areas in the Northern hemisphere calculated form the all season data of Hogben and Lumb (1972) .) The RMS responses calculated for full size vessels of 25.6m (1/16th scale) and 40.0m (1/25th scale) are summarised in Tables 7 to 14.

Several points may be noted from the above tables:

- As might be expected, the RMS motions decrease with increasing vessel size under most conditions; exceptions occur in heave for $S/L = 0.4$ at the highest speed.
- In general the motions of the monohull and catamarans are very similar. Some decrease in pitch response may be noted for the catamarans especially at lower forward speeds. The optimum spacing appears to be dependent on speed since $S/L = 0.4$ gives the lowest pitch response at $F_n = 0.2$, $S/L = 0.2$ at $F_n = 0.5$ and, of the conditions tested, the monohull gives the lowest reponse at $F_n = 0.8$. These trends are also reflected in the forward acceleration responses, which is to be expected since forward acceleration is highly dependent on the pitch response for these long, slender vessels.
- The heave response of the monohull and catamran are similar under all the conditions tested despite the differences in the transfer functions. At the slowest speed tested the catamaran with $S/L = 0.2$ has the minimum response. Similar trends may be found in the RMS LCG acceleration response.

By examining RMS responses in a variety of spectra it is possible to rank the vessels. The striking dissimilarities in the slow speed heave transfer functions become negligible when comparing the RMS responses and it is interesting to note that the more subtle changes in the pitch transfer function have a greater influence in the RMS motions experienced.

5.2 Added resistance

The added resistance for the three models in the various test conditions is given in Figures 134 to 151. The data are plotted to a base of encounter frequency and to a base of $\sqrt{L/\lambda}$. The added resistance has been non-dimensionalised according to Equation 3 noting that B^2/L was the same for monohull and catamaran. The added resistance shows a distinct peak for all the conditions tested; this tends to be the usual form of the added resistance curve for monohulls as can be seen from other published data (see Figure 154).

Some of the results show quite a large amount of scatter and this is particularly true for the results for 4b monohull. The results for model 6b have reduced scatter and this may be due to the increased length and displacement of the model (increasing the magnitude of the forces being measured) when compared with models 4b and 5b.

Some general trends in the results may be deduced together with some exceptions which are also noted:

- In general the magnitude of the catamaran added resistance is approximately twice that of the demihull tested in isolation (monohull). This would be expected if there was no interaction between the demihulls in the catamaran configuration (since two hulls will have twice the added resistance of a single hull). The magnitudes of the results for catamarans with the closer spaced demihulls ($S/L = 0.2$) are slightly less than those with the greater demihull separation. There also appears to be some shifting and broadening of the peak when going from monohull to catamaran. The effect of the second demihull is reduced with increasing $L/\nabla^{\frac{1}{3}}$, which again might be expected.
- The method for non-dimensionalising the added resistance appears to be effective for this hull type since, within certain limits, the results for the different demihulls are unified. Notable exceptions are the results for 4b monohull at $F_n = 0.53$ and 0.8. Here the added resistance is substantially less than the other monohulls (5b and 6b). The results for 4b do however show reasonable agreement with the results of Blok and Beukelman (Figure 154).
- Some of the catamaran results appear to have narrow peaks, and the frequencies at which these appear vary with Froude number, separation and speed.
- For the two finer hull forms — 5b and 6b — the effect of Froude number on added resistance is clearly apparent. The added resistance increases steadily with increasing Froude number and the frequency at which the maximum added resistance occurs increases with speed. This does not appear to hold true for model 4b where there is less speed dependance, especially between the two higher Froude numbers.

6 Comparison with other published data

Little published information is available for catamarans at higher speeds but the the seakeeping properties of the monohulls tested in this work may be compared with those for similar vessels, such as Matsui et al. (1993), Blok and Beukelman (1984) and Faltinsen et al. (1991). The results of this work have been compared with a similar hull form tested by Blok and Beukelman (1984). Comparisons of motions transfer functions are presented in Figures 152 and 153, whilst comparisons of added resistance are made in Figure 154. The models tested in this report do however have somewhat higher length:breadth ratio (9.0–13.1 as compared to 8.0) and this may explain the higher pitch transfer functions. However the same general trends are clearly apparent in the present tests as in those of Blok and Beukelman (1984).

7 Conclusions

The work described in this report covers the experimental determination of the seakeeping properties of monohulls and catamarans based on the NPL round bilge series. Three hull forms have been tested in monohull and two catamaran configurations at three Froude numbers. Measurements of heave pitch and vertical accelerations as well as added resistance due to waves have been made. Several conclusions may be drawn from the experiments:

- The accuracy of the experimental techniques and measurement devices was confirmed by comparison of the measured vertical accelerations and those calculated from the second derivative of vertical motion at the accelerometer positions. Excellent correlation was found for both amplitude and phase of the accelerations.

- The linearity of the response with wave height was assessed for a number of test conditions. A linear relationship was found provided the steepness of the waves was not too large and the motions not too severe. The linear relationship between added resistance and the square of the wave amplitude was also confirmed.

- Response transfer functions were calculated from both regular and irregular wave tests. Excellent correlation was found at low speeds, but this deteriorated at the highest forward speed. This is attributed to the very short run time and hence small number of points obtained from the FFT within the frequency range of interest. The spectra calculated from a number of runs were averaged to try to alleviate this problem but without much success. New experimental and analytical techniques are being developed to try and overcome this problem — see Appendix B. Another possible cause for the observed discrepancies may be due to the linear superposition theory. However it is not clear why since the responses were found to be linear with wave height.

- It is sufficient to discuss only the heave and pitch transfer functions since, as mentioned above, the LCG acceleration was found to correlate very well with the heave, and the forward acceleration was found to be strongly influenced by the pitch. The monohull heave and pitch transfer functions were as expected; at low frequency the motion followed that of the wave, whilst at high frequency little motion was present. A relatively narrow resonant peak was found between these two extremes. The effect of increasing forward speed was to increase the size of the resonant peaks, this effect being most pronounced going from $F_n = 0.2$ to $F_n = 0.5$ with relatively little change in going from $F_n = 0.5$ to $F_n = 0.8$. The forward speed also changed the relative frequencies at which the heave and pitch peaks occurred. The catamaran transfer functions were found to be similar to the monohull. Some broadening of the resonant peak was found, the effect being most pronounced at reduced forward speed. Indeed, for the slowest speed ($F_n = 0.2$), secondary resonant peaks became apparent, especially in heave. A single, large peak was present at the closest demihull spacing ($S/L = 0.2$) and at the wider demihull spacing ($S.L = 0.4$) two smaller peaks were observed. This can be attributed to a greater number of transverse wave modes between the demihulls being present for the wider catamaran.

- Despite the differences in transfer functions between monohull and catamaran, described above, when the RMS motions in several sea states were calculated little difference between the monohull and catamaran was apparent. In most cases the motions for the catamaran were less than for the monohull, when compared on a basis of equal lengths.

- The added resistance was, generally, found to increase with Froude number. The change was greater between $F_n = 0.2$ to 0.5 and much less between $F_n = 0.5$ to 0.8.

- The added resistance of the catamarans was found to be more than twice the monohull value, especially at the higher Froude numbers. It was also discovered that the closer spaced catamaran ($S/L = 0.2$) had less added resistance than the wider catamaran. This may be due to the pitch transfer function for the $S/L = 0.2$ catamaran being less than for the $S/L = 0.4$ catamaran over a substantial part of the frequency range, noting that this was also reflected in the forward acceleration transfer function.

Acknowledgements

The work described in this report forms part of a project funded by EPSRC through the Marine Technology Directorate Ltd under EPSRC Research Grant No. GR/J 50903, MTD Ref. No. MHV 9.

The authors would like to thank the staff in the department of Ship Science and Wolfson Unit MTIA for their assistance during the course of this research. In particular Prof G.J. Goodrich, Mr I.M.C. Campbell, Mr J.L. Robinson and Mr P.A. Weynberg.

References

ABCD working group on human performance at sea (1995). Generating and using human performance simulation data to guide designers and operators of navy ships: Two large multinational programmes. In *International conference on Seakeeping and Weather*, London, England.

Bailey, D. (1976). The NPL high speed round bilge displacement hull series. Maritime Technology Monograph 4, Royal Institution of Naval Architects.

Blok, J. and Beukelman, W. (1984). The high-speed displacement ship systematic series hull forms — seakeeping characteristics. *Trans. The Society of Naval Architects and Marine Engineers.*

BSI (1987). Measurement and evaluation of human exposure to whole-body mechanical vibration and repeated shock. British Standard Guide BS 6841, British Standards Institution.

Clauss, G. and Bergmann, J. (1986). Gaussian wave packets — a new approach to seakeeping tests of ocean structures. *Applied Ocean Research*, 8(4):190–206.

Clauss, G. and Kühnlein, W. (1993). Seakeeping tests with deterministic wave groups and tank side wall wave absorbers. In *20th ITTC*, San Francisco, USA.

Faltinsen, O., Helmers, J., Minsaas, K., and Zhao, R. (1991). Speed loss and operability of catamarans and SES in a seaway. In *Fast '91*, Trondheim, Norway.

Graham, R., Baitis, A., and Meyers, W. (1992). On the development of seakeeping criteria. *Naval Engineers Journal*, 104(3):259–275.

Grigoropoulos, G., Florios, N., and Loukakis, T. (1994). Transient waves for ship and floating structure testing. *Applied Ocean Research*, 16:71–85.

Hogben, N. and Lumb, F. (1967). *Ocean wave statistics.* HMSO.

Insel, M. (1990). *An Investigation into the Resistance Components of High Speed Displacement Catamarans.* PhD thesis, University of Southampton.

Insel, M. and Molland, A. (1992). An investigation into the resistance components of high speed displacement catamarans. *Transactions of the Royal Institution of Naval Architects.*

ISO (1985). Evaluation of human exposure to whole-body vibration — part 3: Evaluation of exposure to whole-body z-axis vertical vibration in the frequency range 0.1 to 0.63 Hz. ISO Report 2631/3, International Organisation for Standardization.

Lloyd, A. (1989). *Seakeeping: Ship Behaviour in Rough Weather.* Series in Marine Technology. Ellis Horwood Limited.

Marwood, W. and Bailey, D. (1969). Design data for high-speed displacement hulls of round-bilge form. Ship Report 99, National Physical Laboratory.

Matsui, S., Shao, S.-M., Wang, Y.-C., and Tanaka, K. (1993). The experimental investigations on resistance and seakeeping qualities of high-speed catamarans. In *Fast '93*, Yokohama, Japan.

Molland, A., Wellicome, J., and Couser, P. (1994). Resistance experiments on a systematic series of high speed displacement catamaran forms: Variation of length-displacement ratio and breadth-draught ratio. Ship Science Report 71, Department of Ship Science, University of Southampton.

Appendix A

A Regular wave analysis

Least squares sine fit For detailed analysis of the regular wave data, including calculating the phase relationships between the motions, a least squares sine fit was developed. The least squares sine fit expects the data to oscillate about zero, thus the first stage of the analysis required a straight line fit to be made to the data ($y = mx + c$). This straight line trend was then removed from the data. The sine fit which was then made to the data is described below:

A first order least squares fit was calculated for the data and this was then removed from the data to produce an oscillation about zero.

The equation which was used for the fit is given in Equation 4.

$$\hat{y} = A1 \sin Bx + A2 \cos Bx \tag{4}$$

Thus the error equation to be minimised is:

$$\sum_i \text{error}^2 = \sum_i (A1 \sin Bx_i + A2 \cos Bx_i - y_i)^2 \tag{5}$$

The coefficients $A1$, $A2$ and B are then found by differentiating Equation 5 with respect to the unknown coefficients and setting the resultant equation equal to zero.

From the differential with respect to $A1$ we obtain Equation 6:

$$2A1 \sum_i \sin^2 Bx_i + A2 \sum_i \sin Bx_i \cos Bx_i - \sum_i y_i \sin Bx_i = 0 \tag{6}$$

and from the differential with respect to $A2$ we obtain Equation 7:

$$2A2 \sum_i \cos^2 Bx_i + A1 \sum_i \sin Bx_i \cos Bx_i - \sum_i y_i \cos Bx_i = 0 \tag{7}$$

finally from the differential with respect to B we obtain Equation 8:

$$\begin{aligned} 2A1^2 \sum_i x_i \sin Bx_i \cos Bx_i - \\ 2A2^2 \sum_i x_i \sin Bx_i \cos Bx_i - \\ A1A2 \sum_i x_i (\cos^2 Bx_i - \sin^2 Bx_i) - \\ A1 \sum_i x_i y_i \cos Bx_i + \\ A2 \sum_i x_i y_i \sin Bx_i \quad = \quad 0 \end{aligned} \tag{8}$$

on defining the following sums:

$$\begin{aligned} \alpha &= \sum_i \sin^2 Bx_i \\ \beta &= \sum_i \cos^2 Bx_i \\ \gamma &= \sum_i \sin Bx_i \cos Bx_i \\ \delta &= \sum_i y_i \sin^2 Bx_i \\ \epsilon &= \sum_i y_i \cos^2 Bx_i \\ \zeta &= \sum_i x_i \sin Bx_i \cos Bx_i \end{aligned}$$

$$\eta = \sum_i x_i(\cos^2 Bx_i - \sin^2 Bx_i)$$
$$\theta = \sum_i x_i y_i \sin Bx_i$$
$$\iota = \sum_i x_i y_i \cos Bx_i$$

Equation 6 becomes:

$$A2 = \frac{\delta - 2A1\alpha}{\gamma} \tag{9}$$

On substituting Equation 9 into Equation 7 and simplifying we get:

$$A1 = \frac{\epsilon\gamma - 2\beta\delta}{\gamma^2 - 4\alpha\beta} \tag{10}$$

and finally Equation 8 becomes:

$$r = 2\zeta(A1^2 - A2^2) + A1A2\eta - A1\iota + A2\theta \tag{11}$$

The coefficients, $A1$, $A2$ and B, are found by assuming a value for B (usually calculated from the zero-crossing period) and iterating Equations 10 and 9 with updated values for B until the residuary r in Equation 11 is reduced to a sufficiently small number.

Appendix B

B Random wave generation

The irregular waves used in the experiments were generated using existing Wolfson Unit MTIA software. Fifty harmonics with random phasing and with regular increments of period are used to generate the required spectra. Whilst this approach proved satisfactory for lower model speeds, there were some shortcomings at higher speeds.

Wave packet and transient wave tests could provide a much faster way of measuring the irregular wave behaviour of a vessel — (Clauss and Kühnlein, 1993) (Clauss and Bergmann, 1986) (Grigoropoulos et al., 1994). These techniques are currently under investigation and may be applied in future experiments.

Appendix C

C Random wave analysis

The irregular wave traces were transformed into the frequency domain using a simple FFT method with a Hanning window. The software was developed by the Wolfson Unit MTIA. Other methods of spectral analysis have been investigated to try and obtain the highest resolution in the frequency range of interest from the short time domain traces. The methods investigated included maximum entropy, maximum likelihood, auto-correlation and different data windowing techniques. However these methods were not found to be particularly successful when used on the very short time series available during the high speed runs.

FFT software The frequency domain spectra were obtained from the time series data by use of a FFT method developed by the Wolfson Unit MTIA. An FFT of the whole time series was carried out (the data either being padded or truncated to obtain a record length containing a number of samples that is an integer power of two). The mean of each trace was removed from the data to produce an oscillation about zero, a Hanning window was then used to reduce leakage. The spectra obtained were normalised using the RMS of the time series data. This method was found to be reasonably successful for slow speed runs where the run time was of reasonable length. However for the high speed runs, where only 4 or 5 seconds of trace were available, several spectra calculated from separate runs were averaged to produce a more stable solution. The other problem with the high speed runs was the high Nyquist frequency which limited the number of FFT points in the frequency range of interest.

Appendix D

D Application of results

As was demonstrated in Section 5.1.2, the transfer functions may be used to determine the ship response to a given sea spectrum. A summary of the method used for calculating the RMS response is given below:

1. Determine the sea spectrum; this is usually defined by a characteristic period (T_0) and significant wave height ($h_{\frac{1}{3}}$). A standard wave spectrum such as ITTC, Jonswap, etc, may then be used to calculate the wave energy at a given frequency: $E_w(\omega)$.

2. The wave energy must be then transformed to a function of encounter frequency (ω_e); see Equation 12. This equation is derived from the fact that the total energy in the spectrum must be the same whether calculated in terms of ω or ω_e.

$$\int_0^\infty E_w(\omega)d\omega = \int_0^\infty E_w(\omega_e)d\omega_e$$

thus,

$$E_w(\omega) = E_w(\omega_e)\frac{d\omega_e}{d\omega}$$

or,

$$E_w(\omega_e) = E_w(\omega).1/\frac{d\omega_e}{d\omega} \tag{12}$$

where, for head seas,

$$\omega_e = \omega + \frac{\omega^2 u}{g}$$

and hence,

$$\frac{d\omega_e}{d\omega} = 1 + \frac{2\omega u}{g}$$

3. The motion spectrum ($M(\omega_e)$) may now be determined from the motion transfer function ($TF(\omega_e)$) and the wave energy spectrum ($E_w(\omega_e)$) — see Equation 13.

$$M(\omega_e) = (TF(\omega_e))^2.E_w(\omega_e) \tag{13}$$

4. For comparison it is usual to calculate the significant motion or RMS motion. This is done by integrating the motion spectrum — see Equation 14.

$$m_0 = \int_0^\infty M(\omega_e)d\omega_e \tag{14}$$

noting that the RMS motion = $\sqrt{m_0}$ and the significant amplitude is twice the RMS motion.

The comparative performance of different vessels may be assessed by examining their RMS or significant responses to a given sea state; as has been done in Section 5.

Table 1: Hull form principal particulars (monohull).

Model:	4b	5b	6b
Length	1.6m	1.6m	2.1m
$L/\nabla^{\frac{1}{3}}$	7.4	8.5	9.5
L/B	9.0	11.0	13.1
B/T	2.0	2.0	2.0
C_B	0.397	0.397	0.397
C_P	0.693	0.693	0.693
C_M	0.565	0.565	0.565
WSA	0.338 m^2	0.276 m^2	0.0.401 m^2
LCB	-6.4%	-6.4%	-6.4%

Note that the longitudinal centre of buoyancy (LCB) is given in percent of ship-length forward of midships.

Table 2: Southampton Institute Tank Details

Length	60m
Breadth	3.7m
Water depth	1.8m
Max carriage speed	4.2 ms^{-1}

Table 3: Relationship between encounter frequency ω_e and ship-length to wavelength ratio L/λ at three Froude numbers.

	Froude Number		
ω_e	0.20	0.50	0.80
6	0.52	0.32	0.24
11	1.33	0.73	0.52
16	2.29	1.23	0.84

Table 4: Wavelength:Model length ratio for the test conditions 1·6m models.

	Encounter Freq. [rads^{-1}]						
F_n	4.0	6.0	8.0	10.0	12.0	14.0	16.0
0.2	3.08	1.97	1.26	0.90	0.69	0.55	0.46
0.5	5.63	3.13	2.09	1.55	1.22	1.00	0.84
0.8	7.31	4.19	2.87	2.16	1.71	1.42	1.21

Table 5: Seakeeping comparison spectra

Spect.	$h_{\frac{1}{3}}$m	T_0 sec	Coef. A	Coef. B
I	2.0	5.0	0.393	0.392
II	2.0	6.5	0.138	0.137
III	2.0	8.0	0.060	0.060

Table 6: Typical all season, all direction sea spectra of the northern hemisphere

Area Code	Sea Area	$h_{\frac{1}{3}}$m	T_0 sec
1	NW Atlantic	4.2	7.1
2	NE Atlantic	4.1	7.2
3	Irish Sea	2.9	5.9
4	North Sea	2.8	5.2
8	Bay of Biscay	1.9	6.7

Table 7: Pitch response for 25.6m vessel, (RMS deg)

S/L	F_n	S I	S II	S III
mono	0.2	7.03	5.45	4.18
mono	0.5	7.20	5.84	4.49
mono	0.8	5.77	5.36	4.32
0.2	0.2	6.43	5.16	4.03
0.2	0.5	6.55	5.47	4.30
0.4	0.2	5.73	4.73	3.76
0.4	0.5	7.20	5.80	4.48
0.4	0.8	6.19	5.49	4.37

Table 8: Pitch response for 40.0m vessel, (RMS deg)

S/L	F_n	S I	S II	S III
mono	0.2	4.96	4.37	3.55
mono	0.5	4.43	4.53	3.80
mono	0.8	2.90	3.73	3.47
0.2	0.2	4.45	4.01	3.35
0.2	0.5	3.98	4.13	3.56
0.4	0.2	3.76	3.60	3.08
0.4	0.5	4.65	4.51	3.37
0.4	0.8	3.41	3.96	3.56

Table 9: Heave response for 25.6m vessel, (RMS m)

S/L	F_n	S I	S II	S III
mono	0.2	0.76	0.91	0.96
mono	0.5	0.94	0.97	0.99
mono	0.8	1.14	1.13	1.08
0.2	0.2	0.71	0.86	0.93
0.2	0.5	0.94	0.97	0.98
0.4	0.2	0.77	0.91	0.96
0.4	0.5	0.93	0.97	0.99
0.4	0.8	1.24	1.20	1.12

Table 10: Heave response for 40.0m vessel, (RMS m)

S/L	F_n	S I	S II	S III
mono	0.2	0.54	0.79	0.90
mono	0.5	0.84	0.94	0.97
mono	0.8	0.91	1.15	1.13
0.2	0.2	0.52	0.73	0.85
0.2	0.5	0.87	0.95	0.97
0.4	0.2	0.54	0.79	0.90
0.4	0.5	0.83	0.93	0.97
0.4	0.8	1.03	1.25	1.21

Table 11: LCG acceleration response for 25.6m vessel, (RMS g)

S/L	F_n	S I	S II	S III
mono	0.2	0.16	0.13	0.10
mono	0.5	0.55	0.40	0.29
mono	0.8	0.80	0.62	0.46
0.2	0.2	0.18	0.14	0.11
0.2	0.5	0.55	0.40	0.29
0.4	0.2	0.16	0.13	0.10
0.4	0.5	0.62	0.44	0.32
0.4	0.8	0.91	0.69	0.51

Table 12: LCG acceleration response for 40.0m vessel, (RMS g)

S/L	F_n	S I	S II	S III
mono	0.2	0.10	0.10	0.09
mono	0.5	0.39	0.34	0.26
mono	0.8	0.49	0.50	0.41
0.2	0.2	0.12	0.11	0.09
0.2	0.5	0.41	0.34	0.26
0.4	0.2	0.10	0.10	0.09
0.4	0.5	0.46	0.38	0.29
0.4	0.8	0.57	0.57	0.45

Table 13: Forward acceleration response for 25.6m vessel, (RMS g)

S/L	F_n	S I	S II	S III
mono	0.2	0.54	0.36	0.25
mono	0.5	1.29	0.91	0.64
mono	0.8	1.35	1.06	0.77
0.2	0.2	0.56	0.37	0.26
0.2	0.5	1.19	0.84	0.59
0.4	0.2	0.50	0.33	0.23
0.4	0.5	1.41	0.97	0.68
0.4	0.8	1.47	1.12	0.81

Table 14: Forward acceleration response for 40.0m vessel, (RMS g)

S/L	F_n	S I	S II	S III
mono	0.2	0.45	0.33	0.24
mono	0.5	0.92	0.79	0.59
mono	0.8	0.82	0.85	0.69
0.2	0.2	0.47	0.34	0.24
0.2	0.5	0.87	0.73	0.55
0.4	0.2	0.42	0.30	0.22
0.4	0.5	1.06	0.86	0.64
0.4	0.8	0.93	0.92	0.73

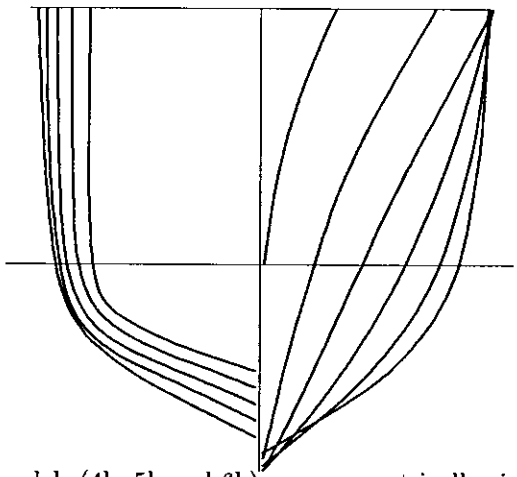

Note: The body plans of all models (4b, 5b and 6b) were geometrically similar and had $B/T = 2.0$

Figure 1: Model 4b, 5b and 6b — Body plan.

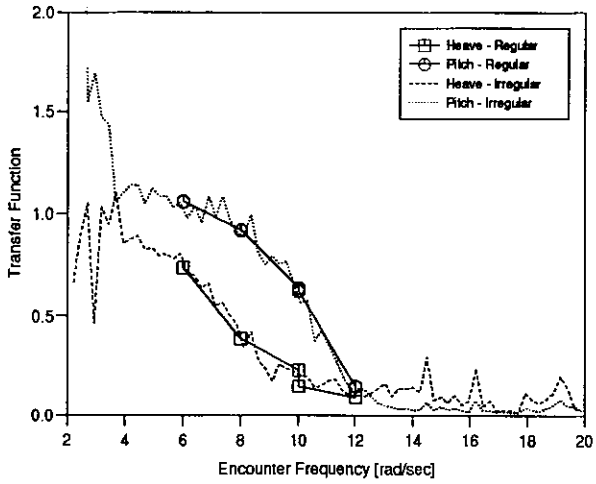

Figure 2: Model 4b Monohull, $F_n = 0.2$ — Heave and Pitch

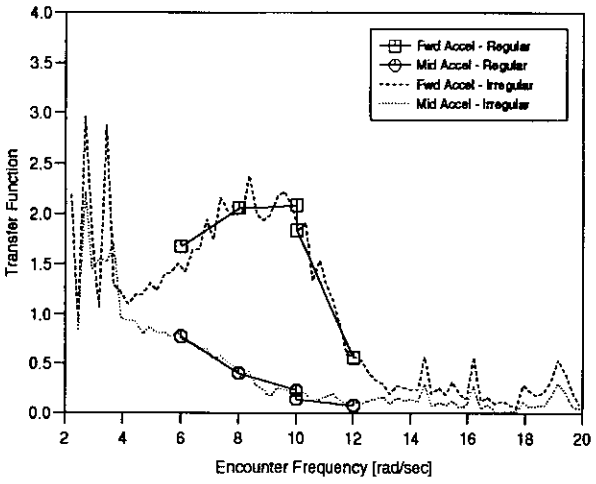

Figure 3: Model 4b Monohull, $F_n = 0.2$ — Accelerations

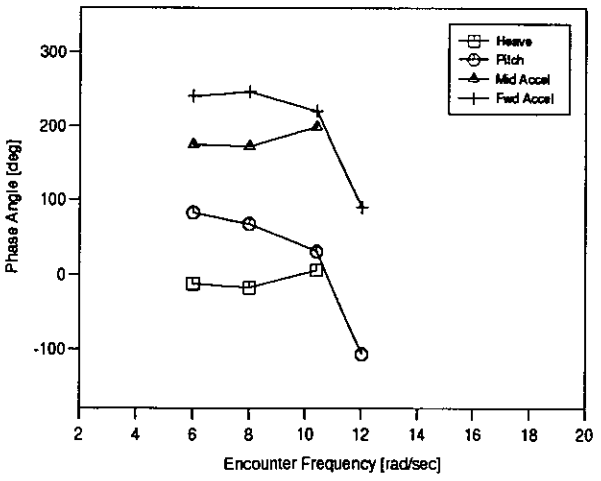

Figure 4: Model 4b Monohull, $F_n = 0.2$ — Phase

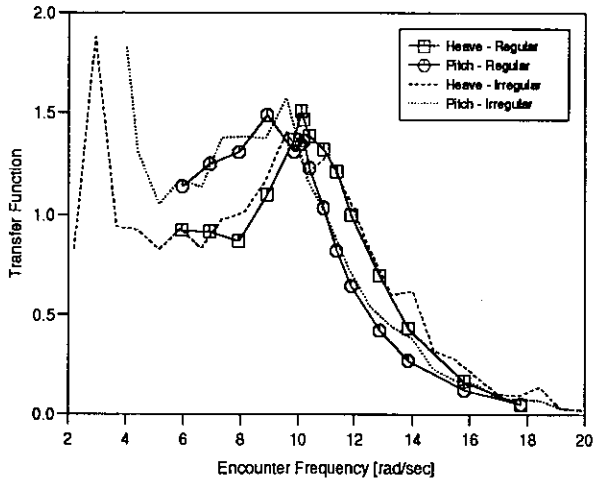

Figure 5: Model 4b Monohull, $F_n = 0.53$ — Heave and Pitch

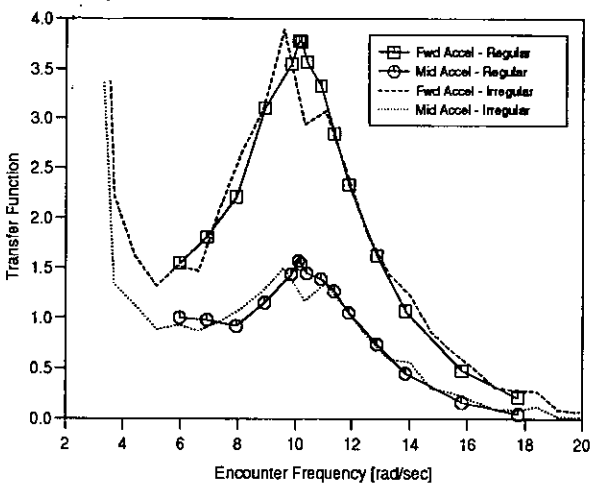

Figure 6: Model 4b Monohull, $F_n = 0.53$ — Accelerations

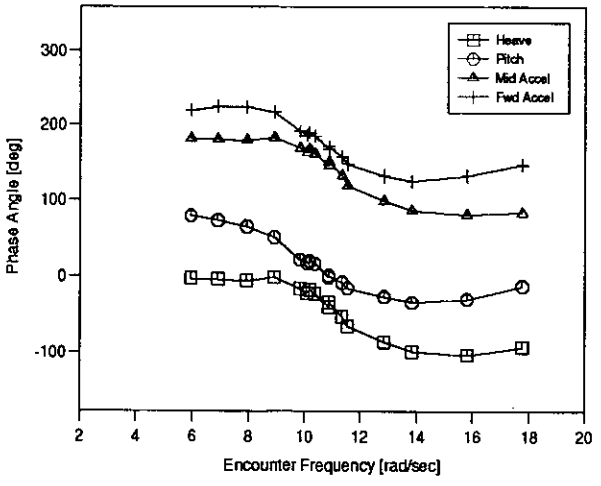

Figure 7: Model 4b Monohull, $F_n = 0.53$ — Phase

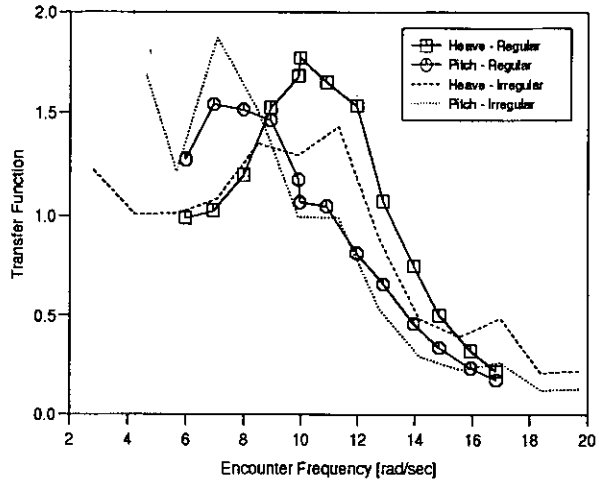

Figure 8: Model 4b Monohull, $F_n = 0.8$ — Heave and Pitch

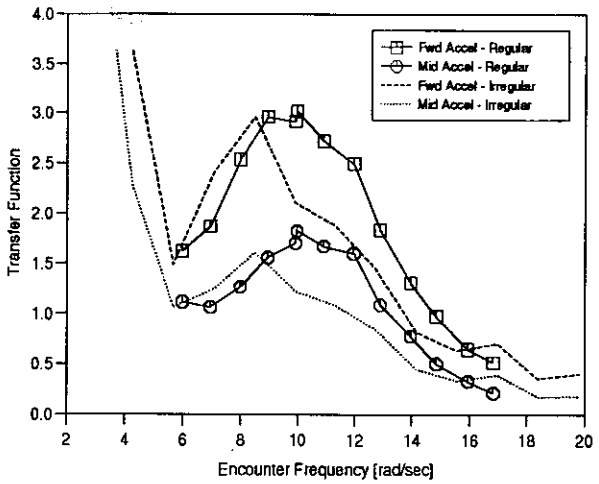

Figure 9: Model 4b Monohull, $F_n = 0.8$ — Accelerations

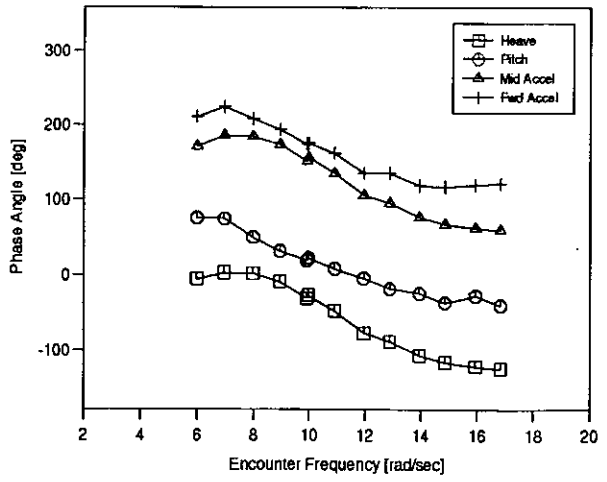

Figure 10: Model 4b Monohull, $F_n = 0.8$ — Phase

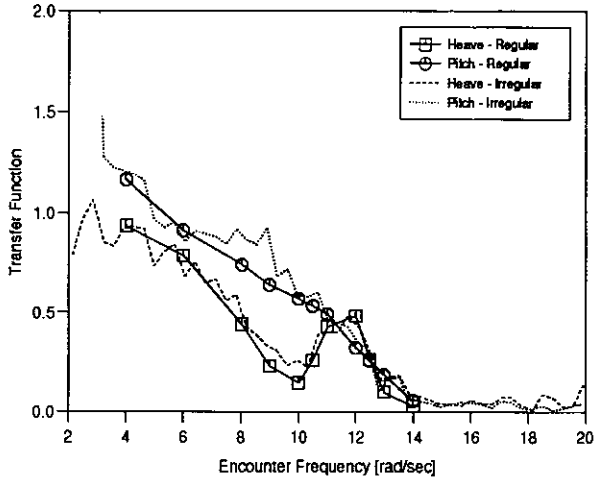

Figure 11: Model 4b $S/L = 0.2$, $F_n = 0.2$ — Heave and Pitch

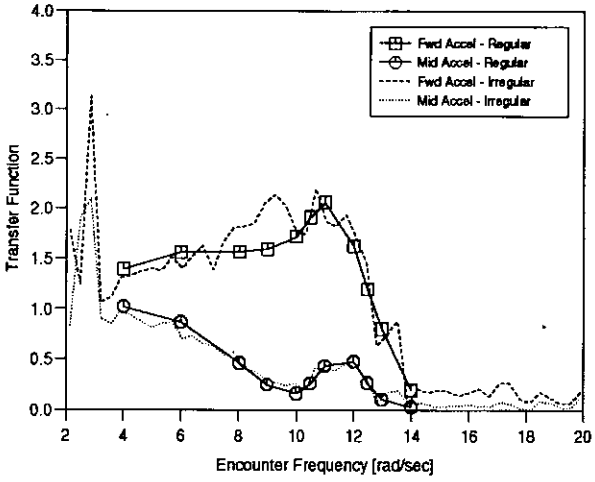

Figure 12: Model 4b $S/L = 0.2$, $F_n = 0.2$ — Accelerations

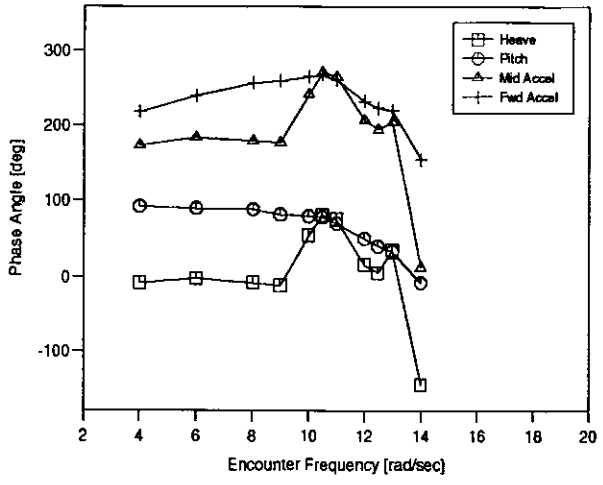

Figure 13: Model 4b $S/L = 0.2$, $F_n = 0.2$ — Phase

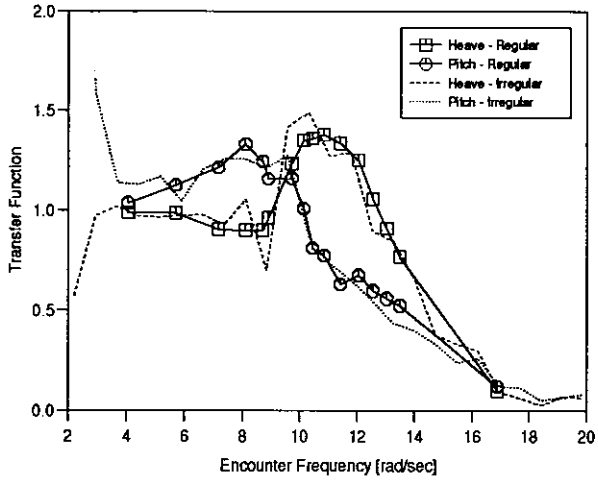

Figure 14: Model 4b $S/L = 0.2$, $F_n = 0.53$ — Heave and Pitch

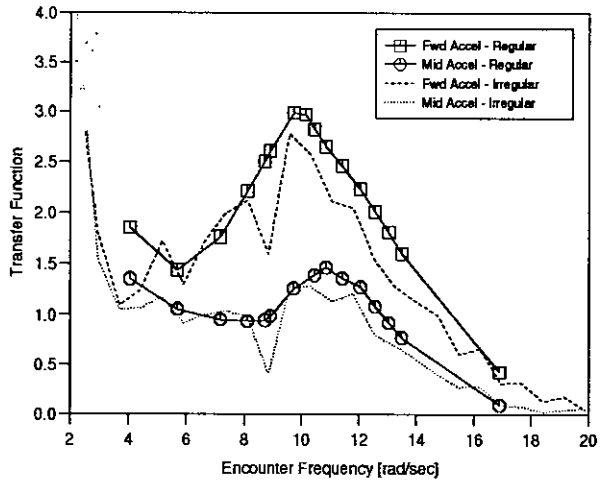

Figure 15: Model 4b $S/L = 0.2$, $F_n = 0.53$ — Accelerations

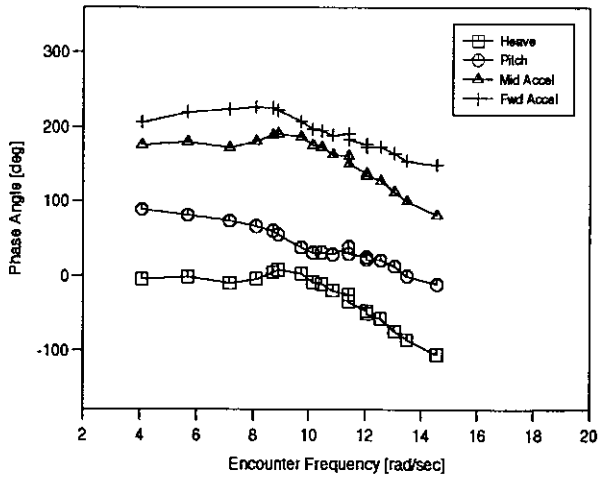

Figure 16: Model 4b $S/L = 0.2$, $F_n = 0.53$ — Phase

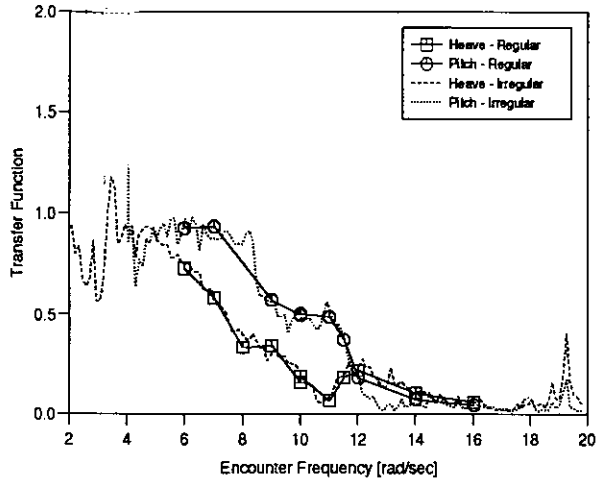

Figure 17: Model 4b $S/L = 0.4$, $F_n = 0.2$ — Heave and Pitch

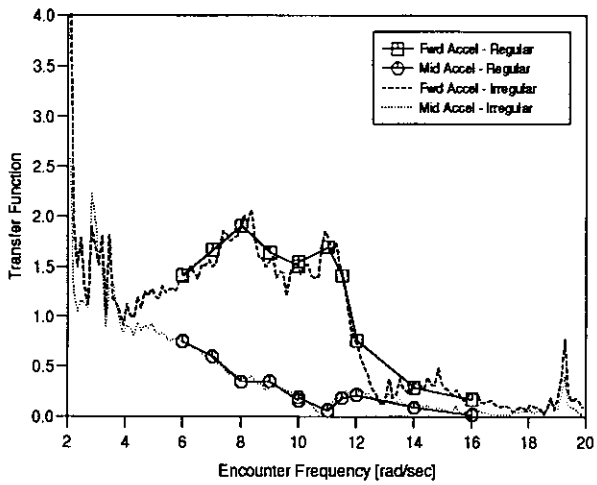

Figure 18: Model 4b $S/L = 0.4$, $F_n = 0.2$ — Accelerations

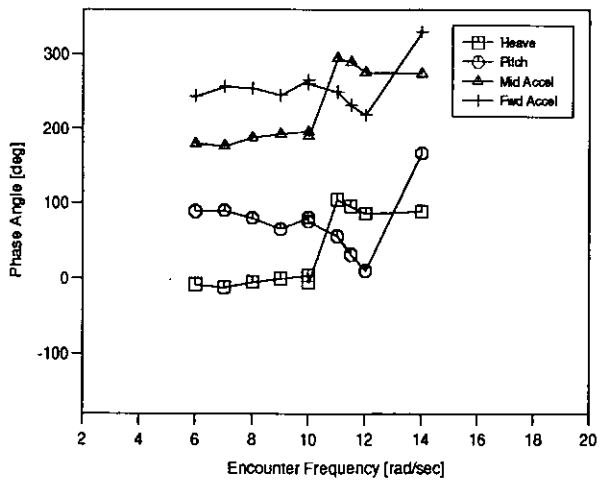

Figure 19: Model 4b $S/L = 0.4$, $F_n = 0.2$ — Phase

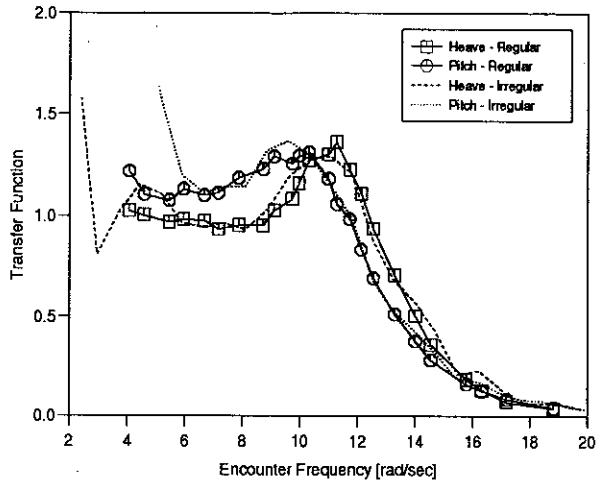

Figure 20: Model 4b $S/L = 0.4$, $F_n = 0.53$ — Heave and Pitch

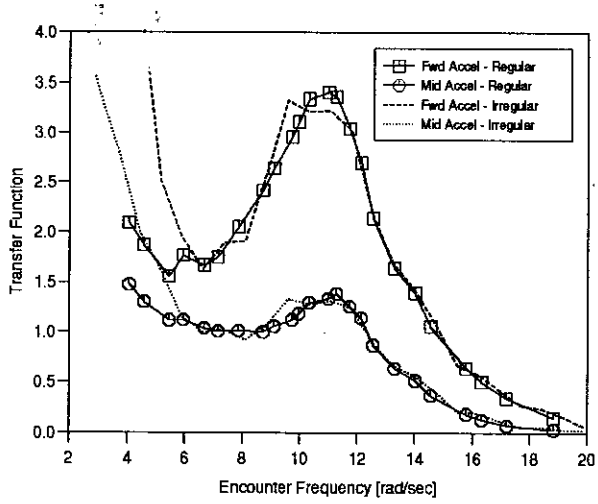

Figure 21: Model 4b $S/L = 0.4$, $F_n = 0.53$ — Accelerations

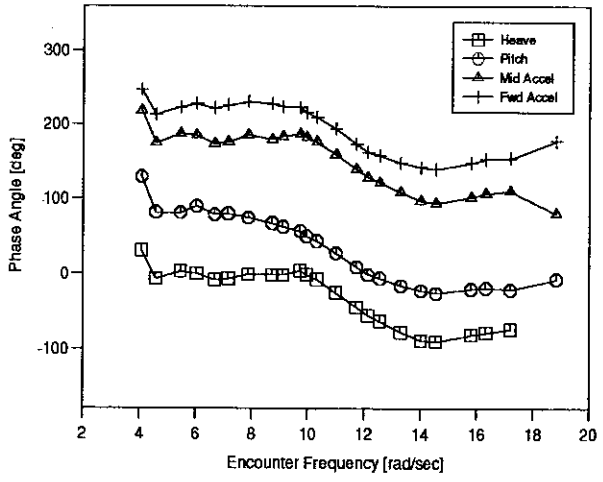

Figure 22: Model 4b $S/L = 0.4$, $F_n = 0.53$ — Phase

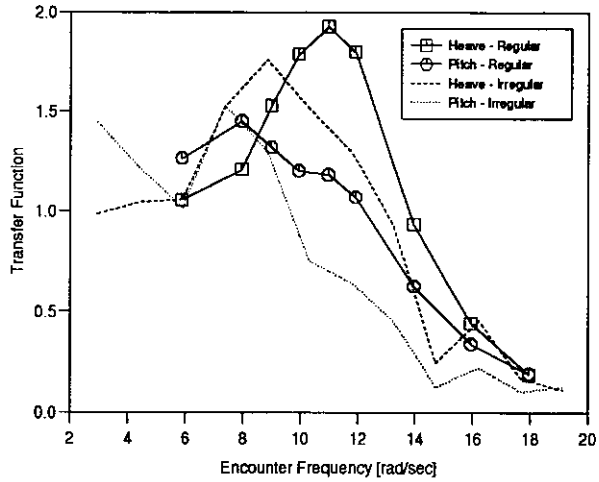

Figure 23: Model 4b $S/L = 0.4$, $F_n = 0.8$ — Heave and Pitch

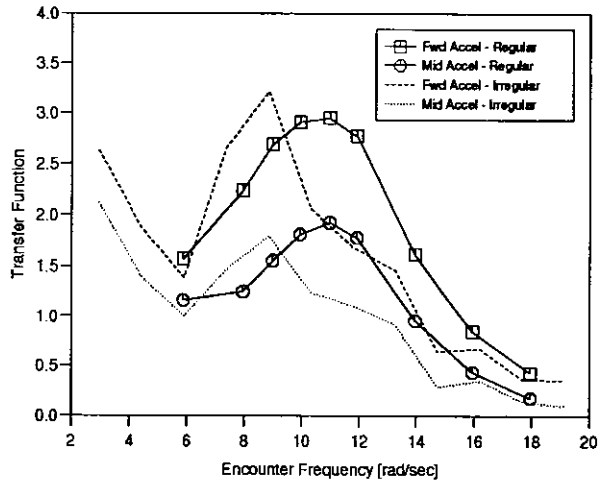

Figure 24: Model 4b $S/L = 0.4$, $F_n = 0.8$ — Accelerations

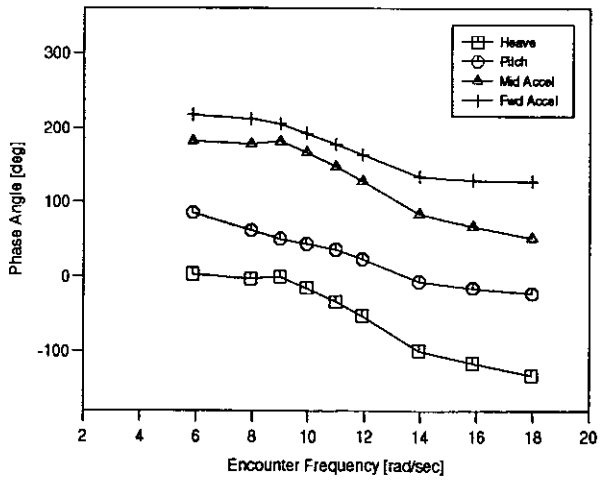

Figure 25: Model 4b $S/L = 0.4$, $F_n = 0.8$ — Phase

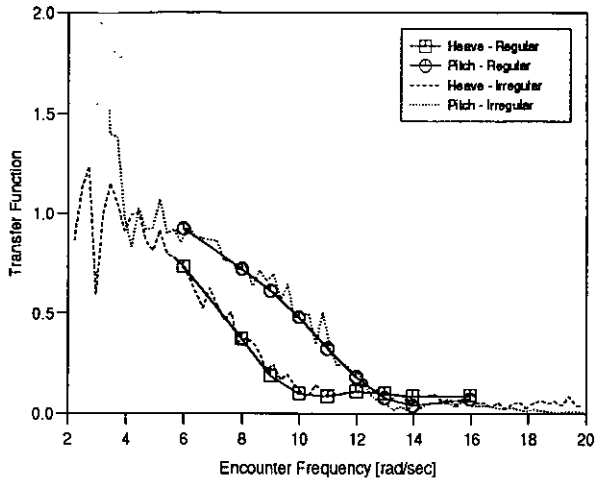

Figure 26: Model 5b Monohull, $Fn = 0.2$ — Heave and Pitch

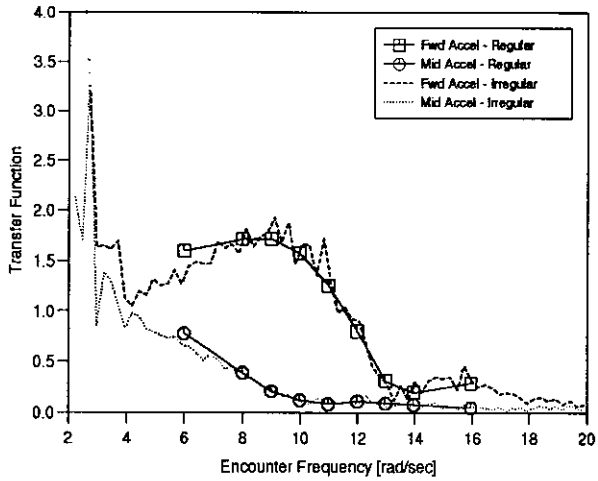

Figure 27: Model 5b Monohull, $Fn = 0.2$ — Accelerations

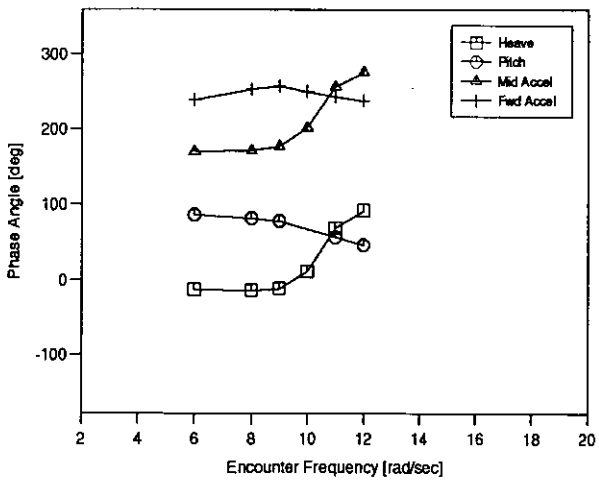

Figure 28: Model 5b Monohull, $Fn = 0.2$ — Phase

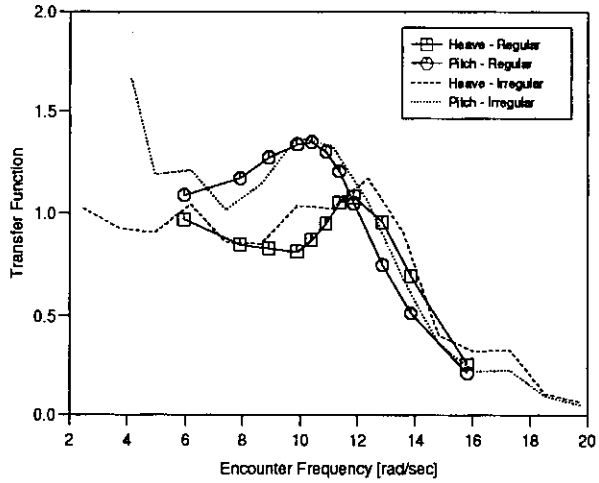

Figure 29: Model 5b Monohull, $Fn = 0.53$ — Heave and Pitch

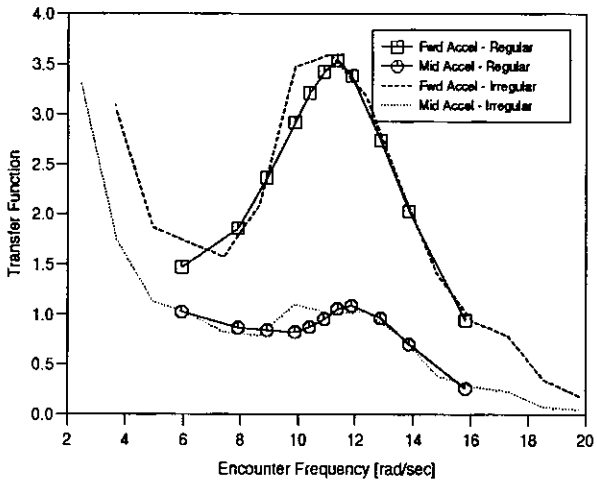

Figure 30: Model 5b Monohull, $Fn = 0.53$ — Accelerations

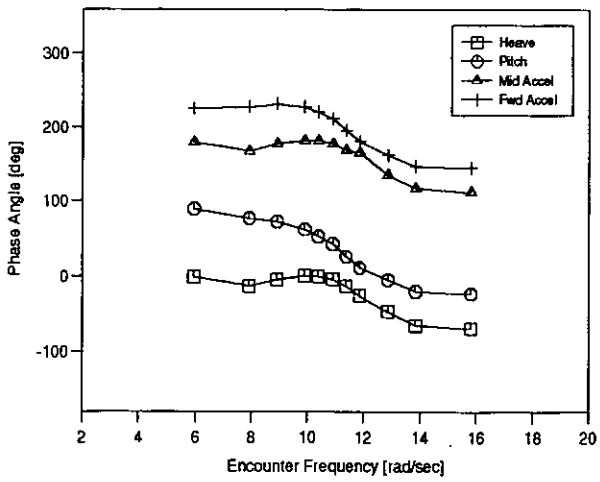

Figure 31: Model 5b Monohull, $Fn = 0.53$ — Phase

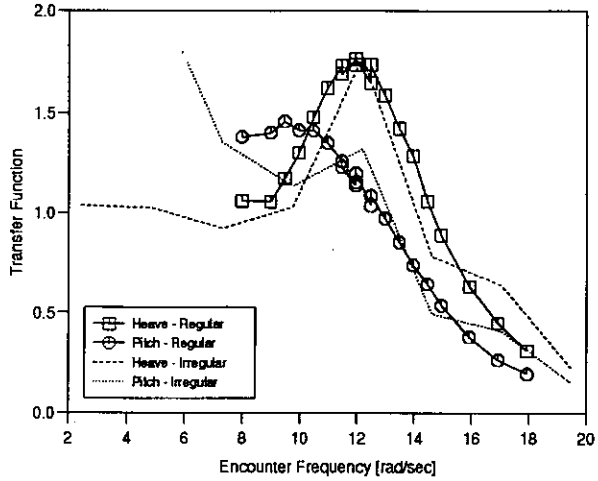

Figure 32: Model 5b Monohull, $Fn = 0.8$ — Heave and Pitch

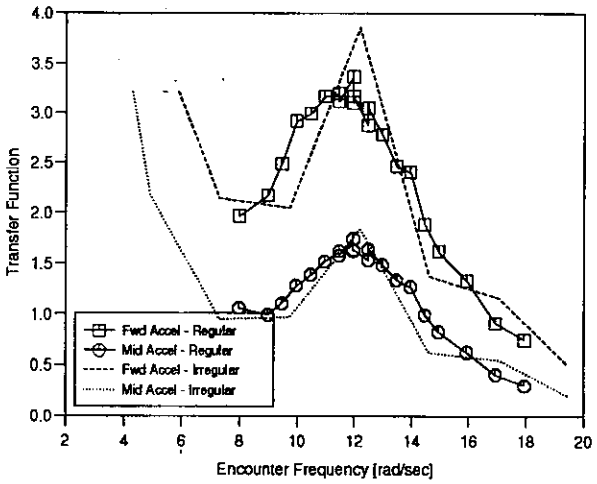

Figure 33: Model 5b Monohull, $Fn = 0.8$ — Accelerations

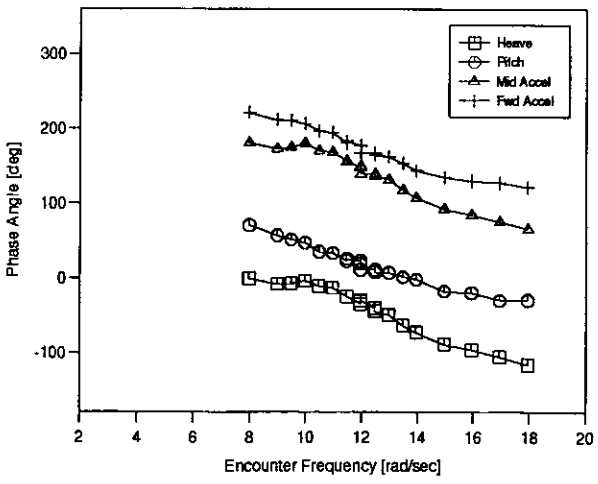

Figure 34: Model 5b Monohull, $Fn = 0.8$ — Phase

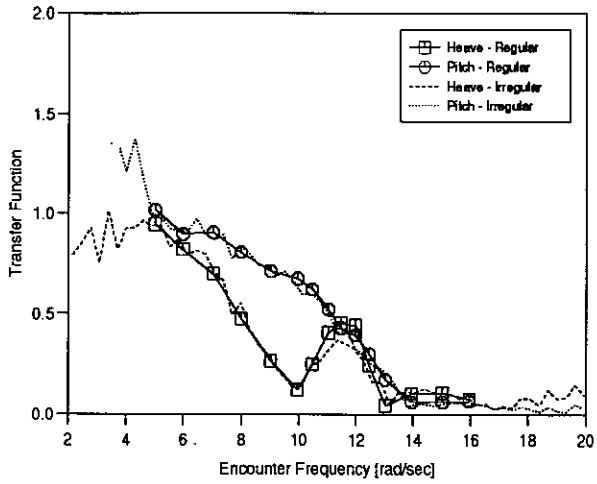

Figure 35: Model 5b $S/L = 0.2$, $Fn = 0.2$ — Heave and Pitch

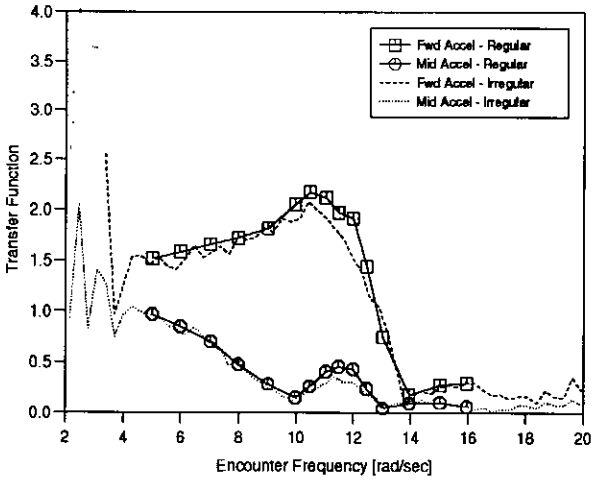

Figure 36: Model 5b $S/L = 0.2$, $Fn = 0.2$ — Accelerations

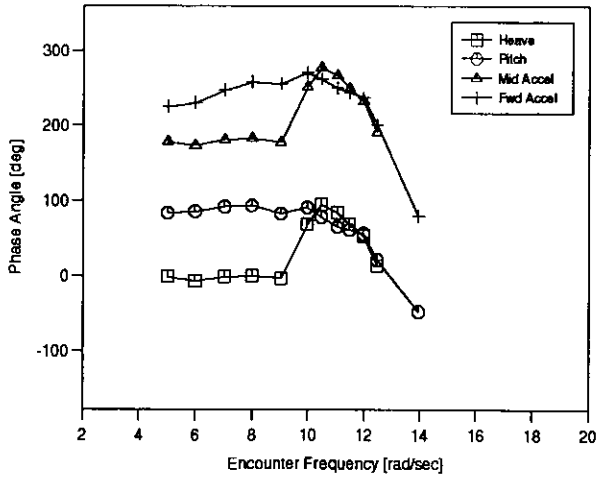

Figure 37: Model 5b $S/L = 0.2$, $Fn = 0.2$ — Phase

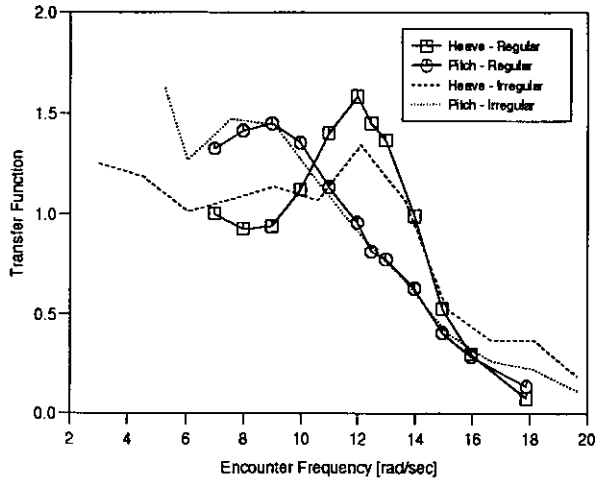

Figure 38: Model 5b $S/L = 0.2$, $Fn = 0.53$ — Heave and Pitch

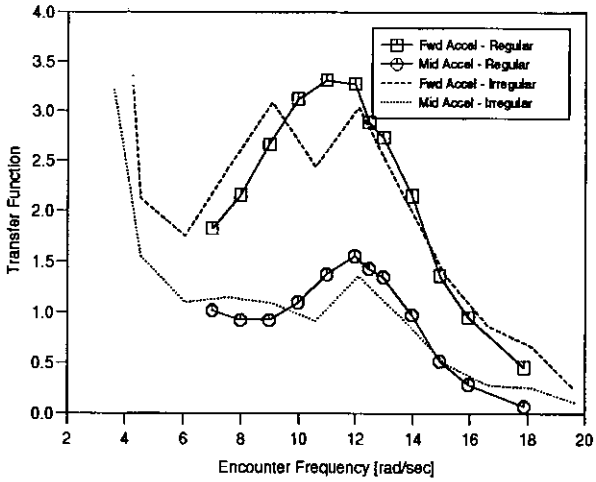

Figure 39: Model 5b $S/L = 0.2$, $Fn = 0.53$ — Accelerations

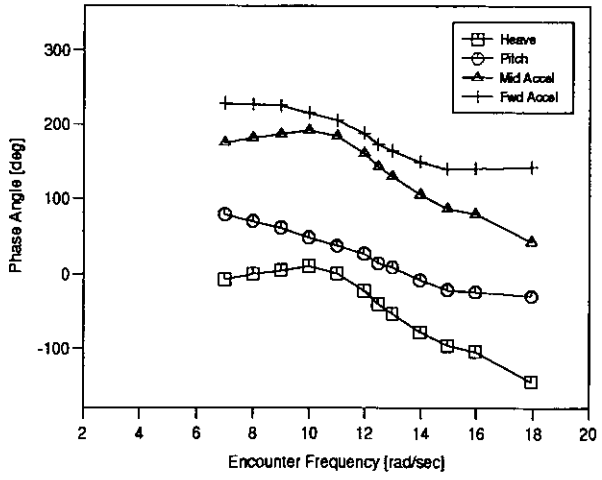

Figure 40: Model 5b $S/L = 0.2$, $Fn = 0.53$ — Phase

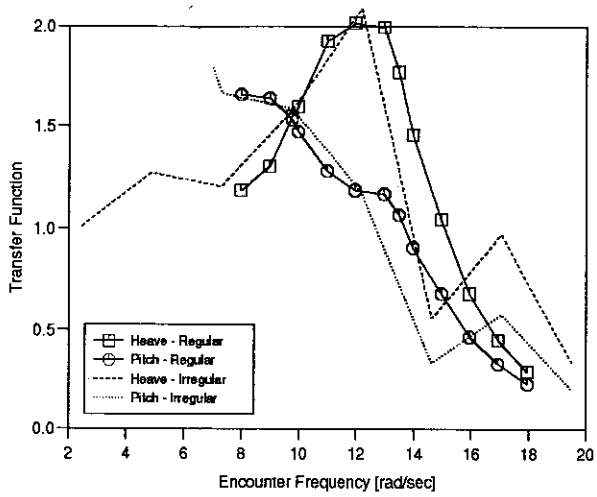

Figure 41: Model 5b $S/L = 0.2$, $Fn = 0.8$ — Heave and Pitch

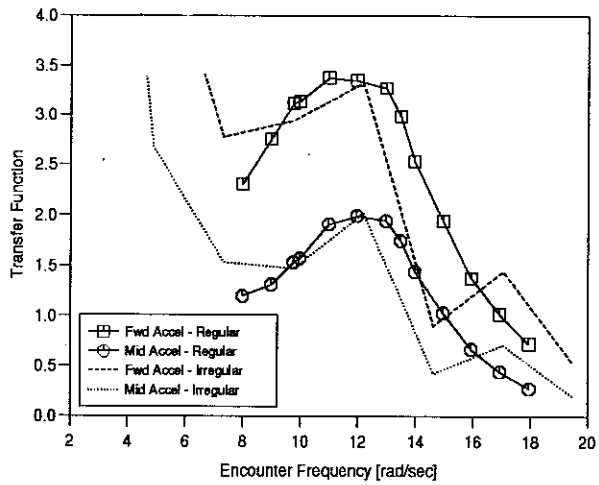

Figure 42: Model 5b $S/L = 0.2$, $Fn = 0.8$ — Accelerations

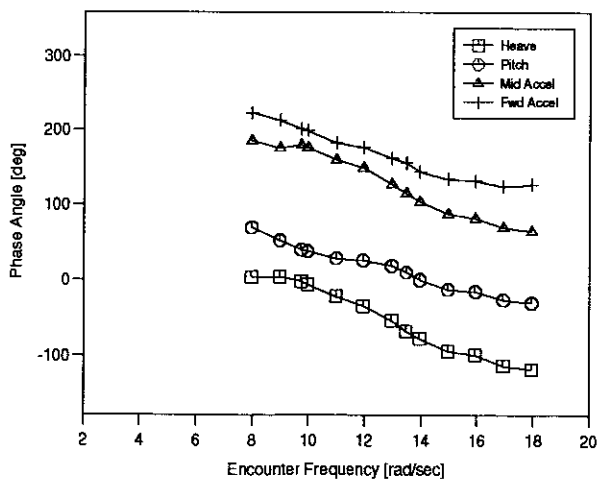

Figure 43: Model 5b $S/L = 0.2$, $Fn = 0.8$ — Phase

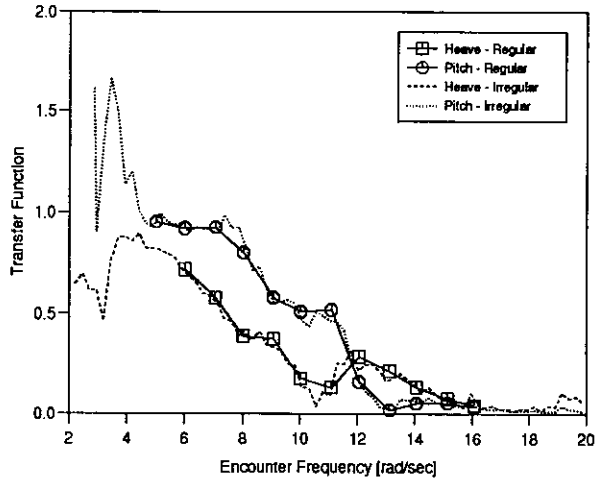

Figure 44: Model 5b $S/L = 0.4$, $Fn = 0.2$ — Heave and Pitch

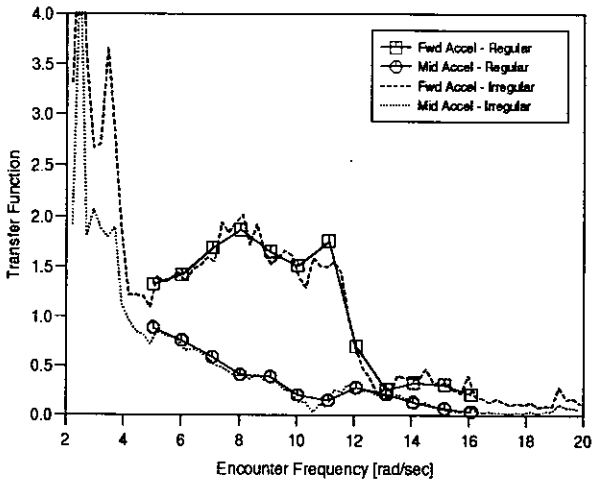

Figure 45: Model 5b $S/L = 0.4$, $Fn = 0.2$ — Accelerations

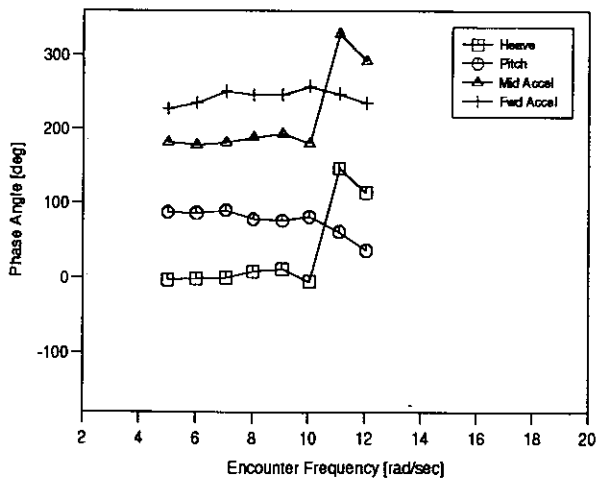

Figure 46: Model 5b $S/L = 0.4$, $Fn = 0.2$ — Phase

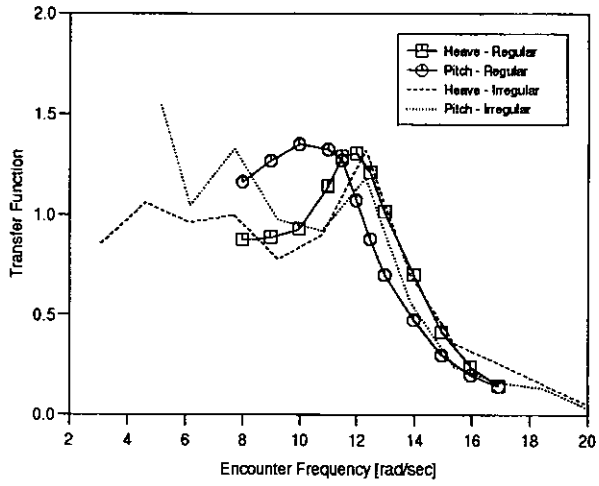

Figure 47: Model 5b $S/L = 0.4$, $Fn = 0.53$ — Heave and Pitch

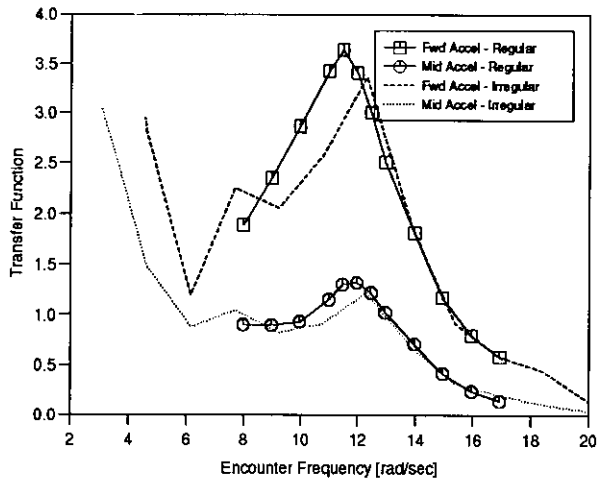

Figure 48: Model 5b $S/L = 0.4$, $Fn = 0.53$ — Accelerations

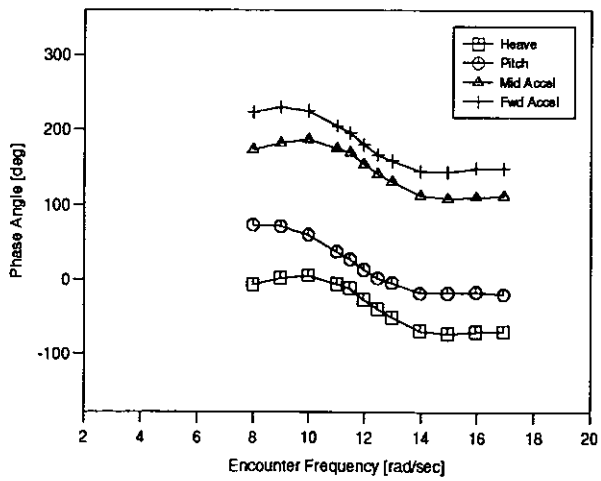

Figure 49: Model 5b $S/L = 0.4$, $Fn = 0.53$ — Phase

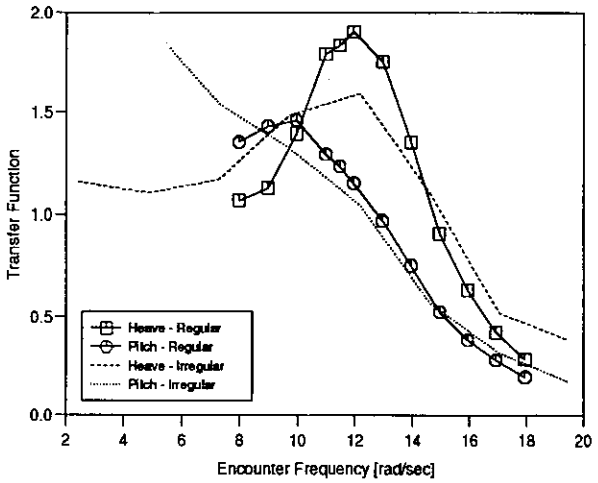

Figure 50: Model 5b $S/L = 0.4$, $Fn = 0.8$ — Heave and Pitch

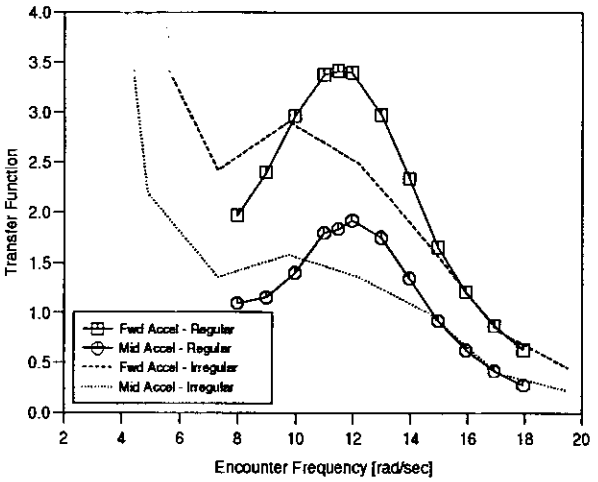

Figure 51: Model 5b $S/L = 0.4$, $Fn = 0.8$ — Accelerations

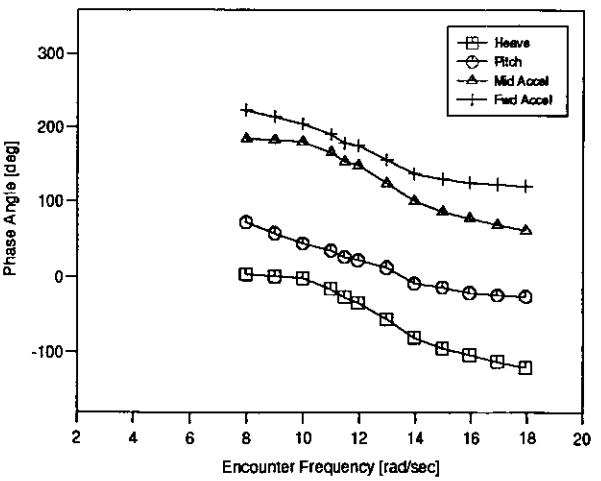

Figure 52: Model 5b $S/L = 0.4$, $Fn = 0.8$ — Phase

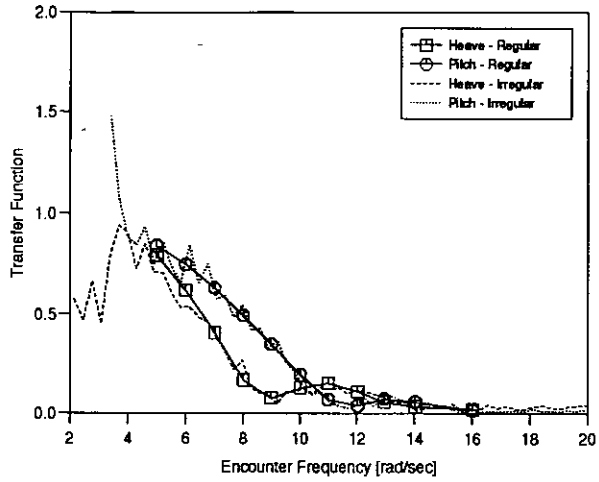

Figure 53: Model 6b Monohull, $Fn = 0.2$ — Heave and Pitch

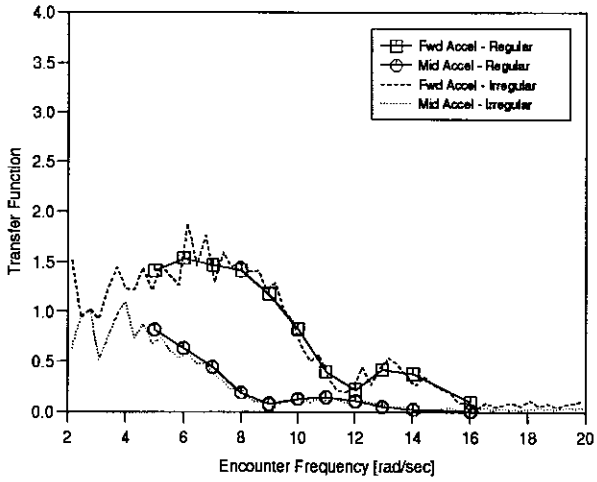

Figure 54: Model 6b Monohull, $Fn = 0.2$ — Accelerations

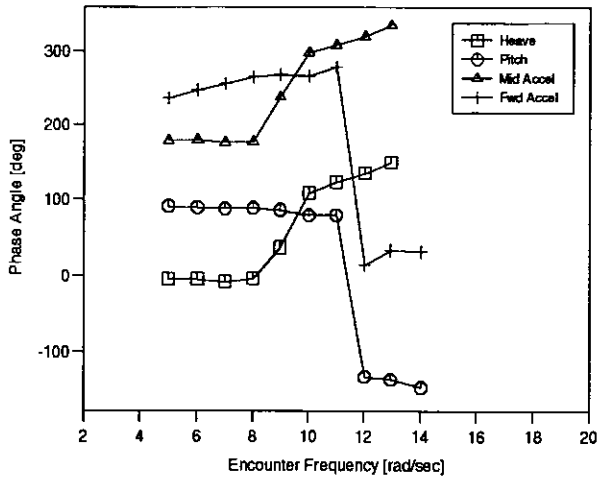

Figure 55: Model 6b Monohull, $Fn = 0.2$ — Phase

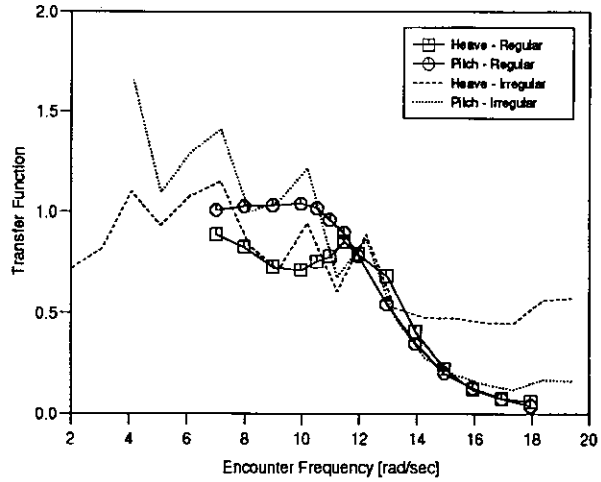

Figure 56: Model 6b Monohull, $Fn = 0.53$ — Heave and Pitch

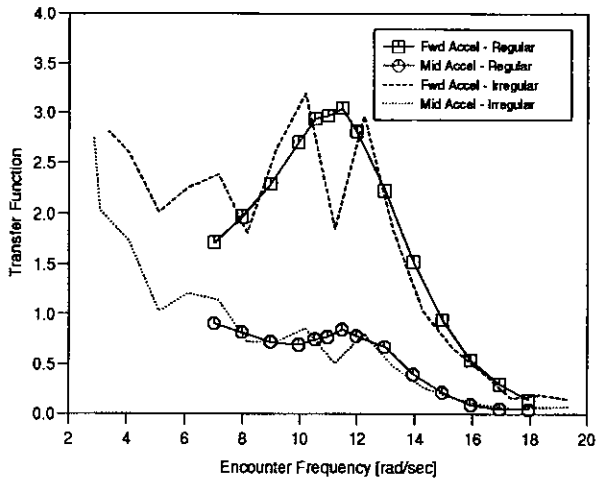

Figure 57: Model 6b Monohull, $Fn = 0.53$ — Accelerations

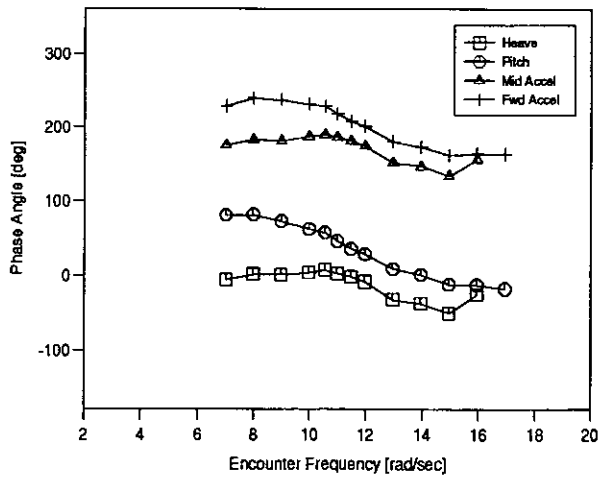

Figure 58: Model 6b Monohull, $Fn = 0.53$ — Phase

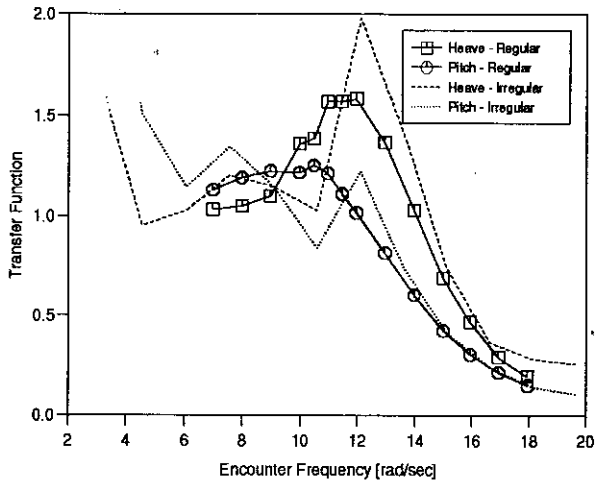

Figure 59: Model 6b Monohull, $Fn = 0.8$ — Heave and Pitch

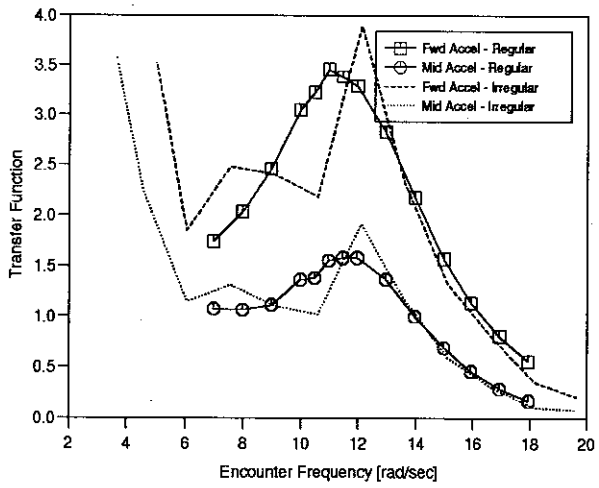

Figure 60: Model 6b Monohull, $Fn = 0.8$ — Accelerations

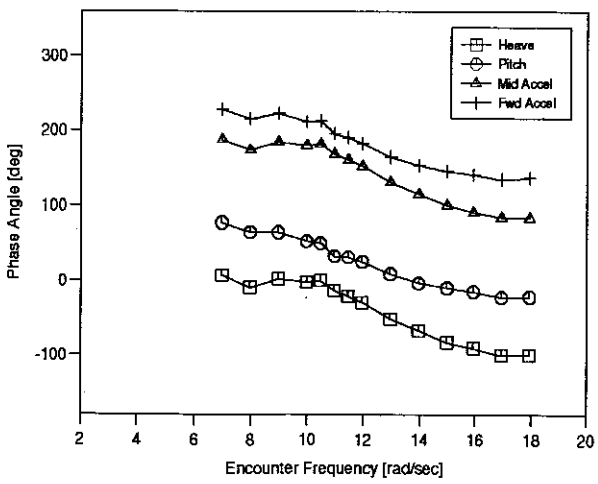

Figure 61: Model 6b Monohull, $Fn = 0.8$ — Phase

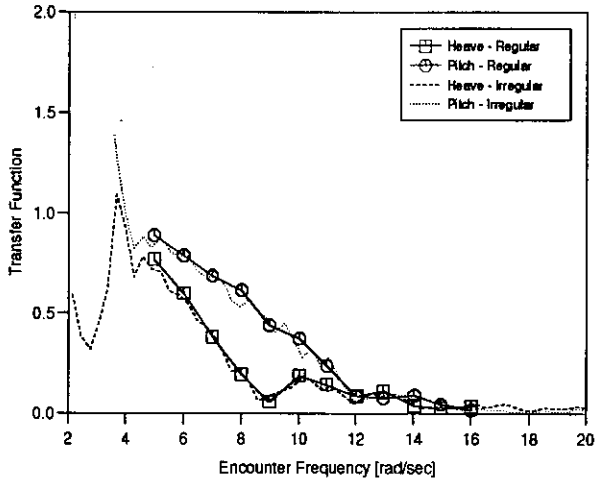

Figure 62: Model 6b $S/L = 0.2$, $Fn = 0.2$ — Heave and Pitch

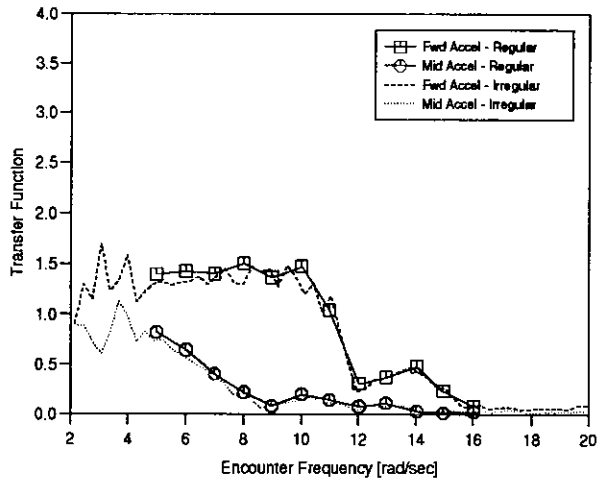

Figure 63: Model 6b $S/L = 0.2$, $Fn = 0.2$ — Accelerations

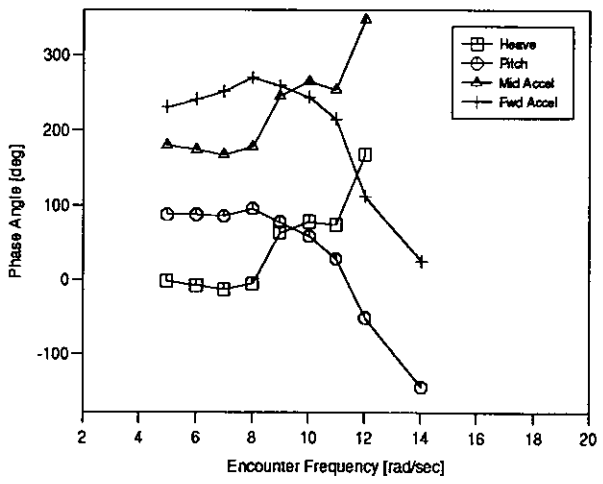

Figure 64: Model 6b $S/L = 0.2$, $Fn = 0.2$ — Phase

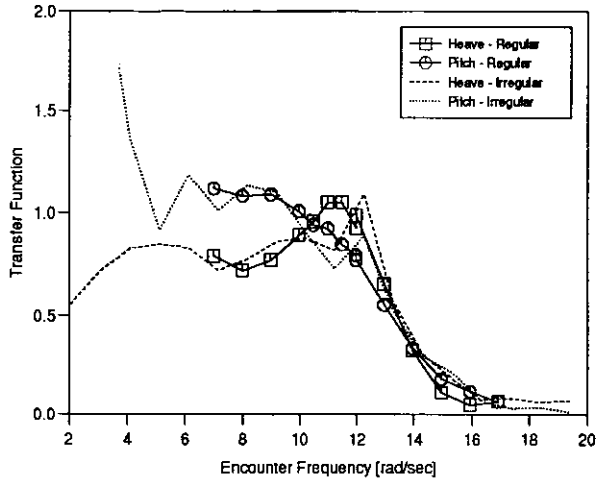

Figure 65: Model 6b $S/L = 0.2$, $Fn = 0.53$ — Heave and Pitch

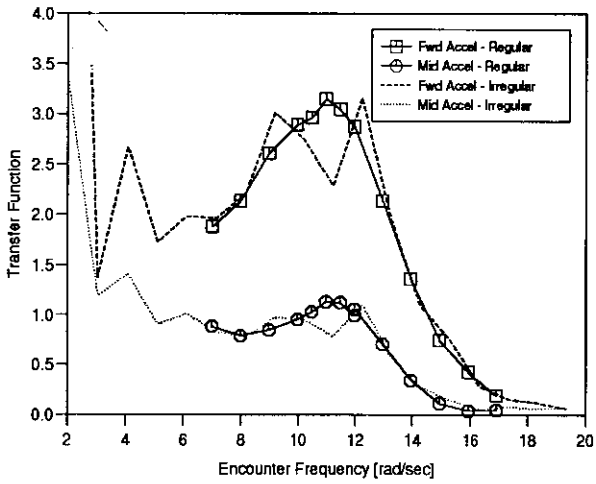

Figure 66: Model 6b $S/L = 0.2$, $Fn = 0.53$ — Accelerations

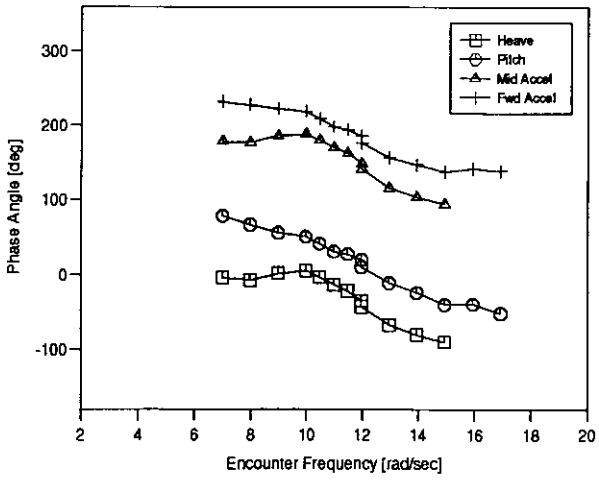

Figure 67: Model 6b $S/L = 0.2$, $Fn = 0.53$ — Phase

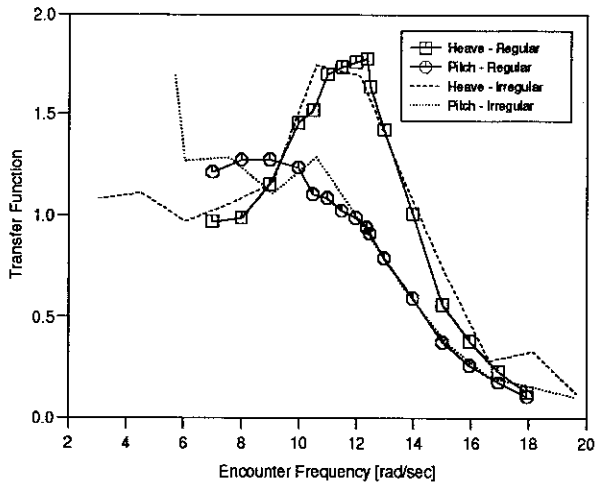

Figure 68: Model 6b $S/L = 0.2$, $Fn = 0.8$ — Heave and Pitch

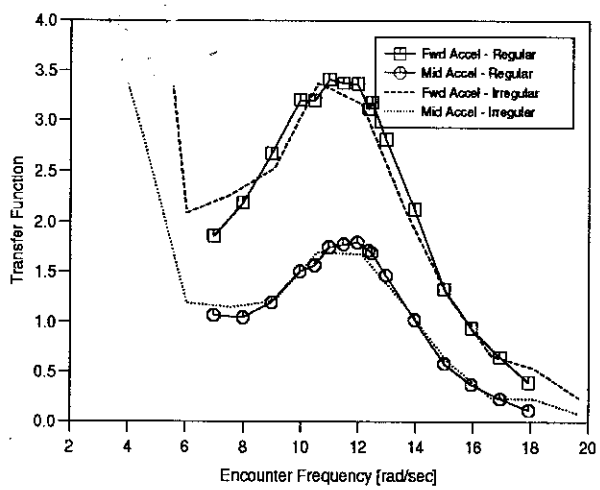

Figure 69: Model 6b $S/L = 0.2$, $Fn = 0.8$ — Accelerations

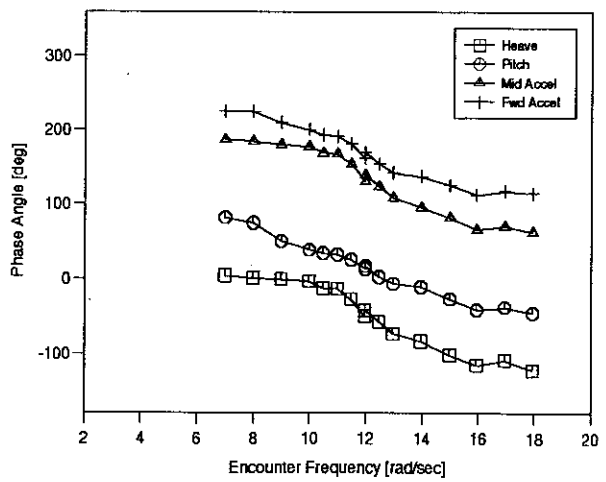

Figure 70: Model 6b $S/L = 0.2$, $Fn = 0.8$ — Phase

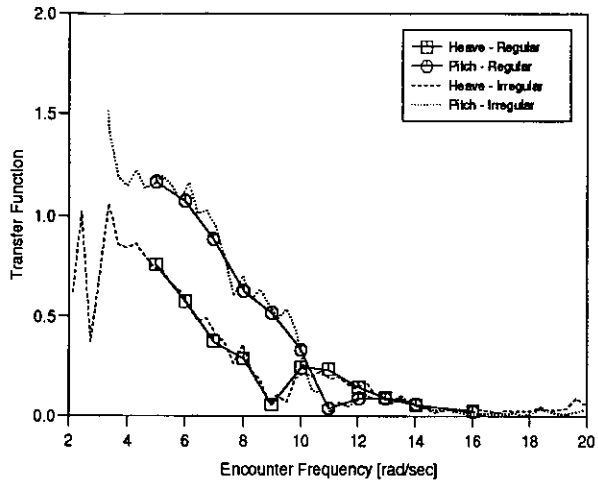

Figure 71: Model 6b $S/L = 0.4$, $Fn = 0.2$ — Heave and Pitch

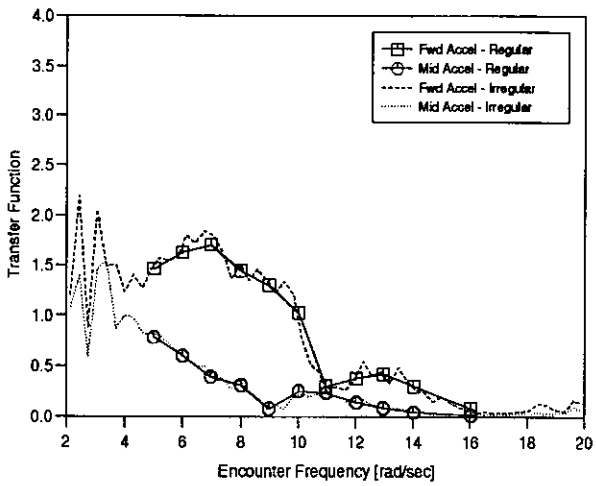

Figure 72: Model 6b $S/L = 0.4$, $Fn = 0.2$ — Accelerations

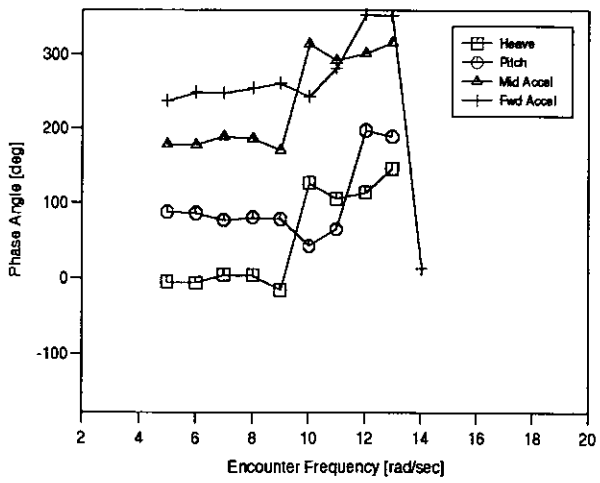

Figure 73: Model 6b $S/L = 0.4$, $Fn = 0.2$ — Phase

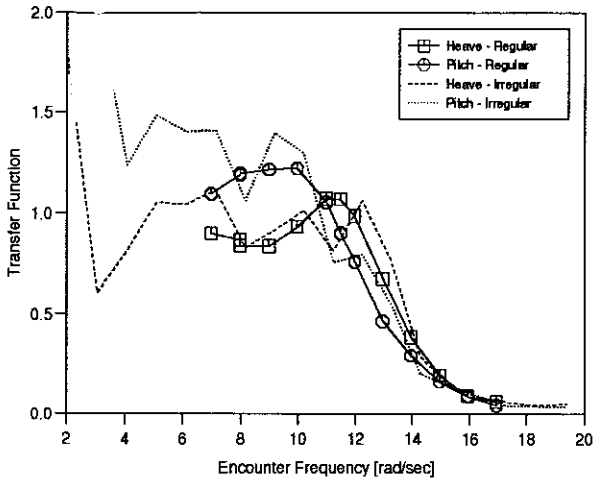

Figure 74: Model 6b $S/L = 0.4$, $Fn = 0.53$ — Heave and Pitch

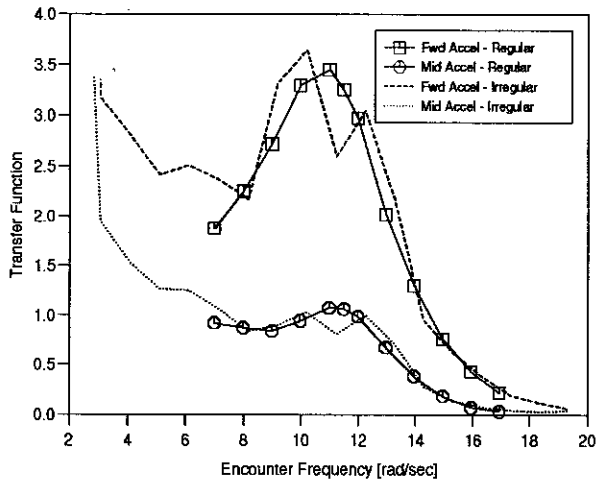

Figure 75: Model 6b $S/L = 0.4$, $Fn = 0.53$ — Accelerations

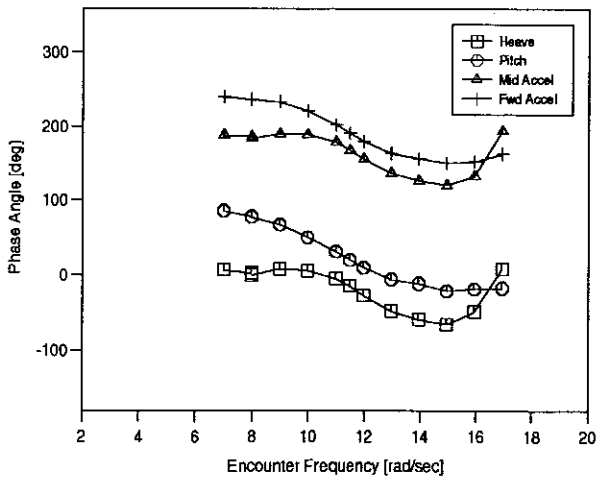

Figure 76: Model 6b $S/L = 0.4$, $Fn = 0.53$ — Phase

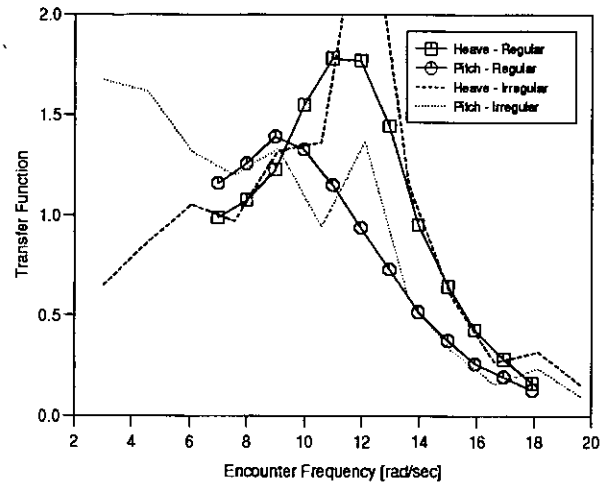

Figure 77: Model 6b $S/L = 0.4$, $Fn = 0.8$ — Heave and Pitch

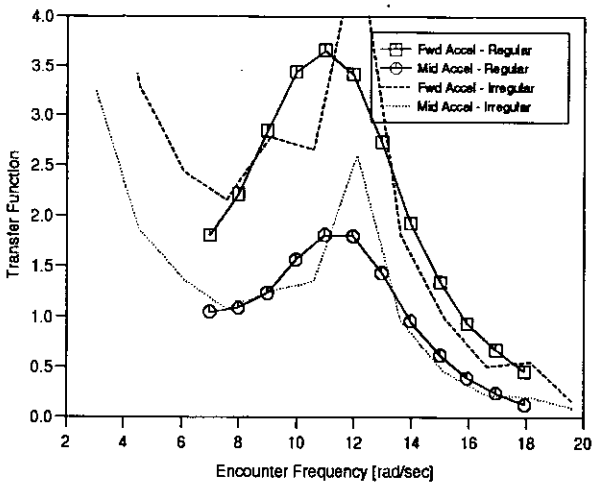

Figure 78: Model 6b $S/L = 0.4$, $Fn = 0.8$ — Accelerations

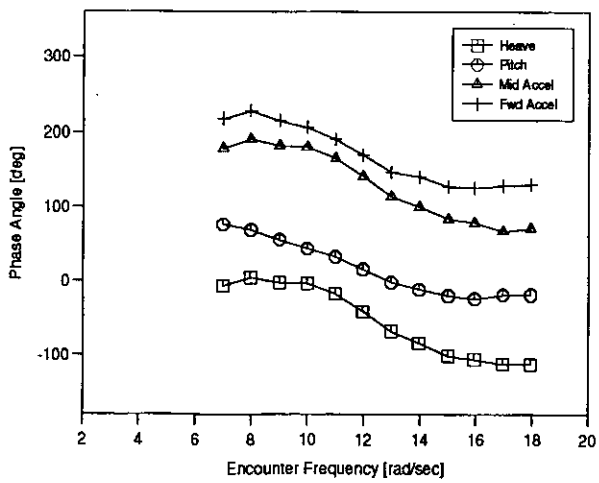

Figure 79: Model 6b $S/L = 0.4$, $Fn = 0.8$ — Phase

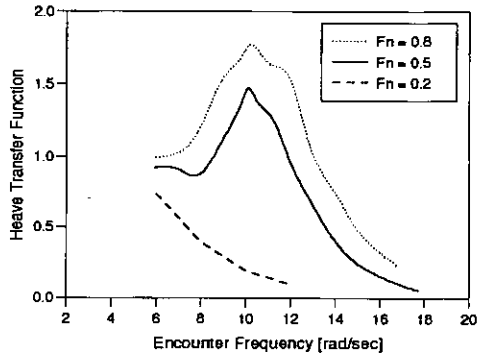

Figure 80a: Heave

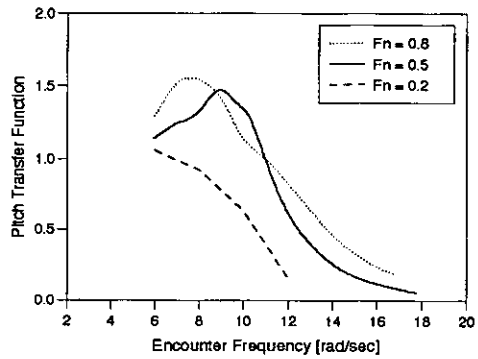

Figure 80b: Pitch

Figure 80: Model 4b Monohull, Effect of F_n on Heave and Pitch

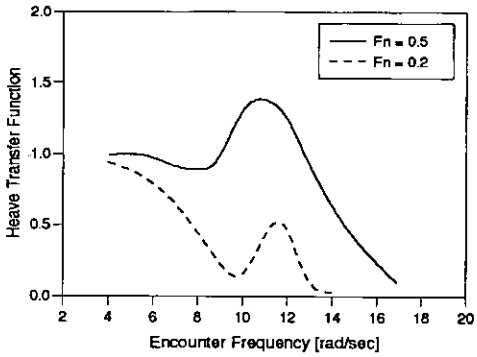

Figure 81a: Heave

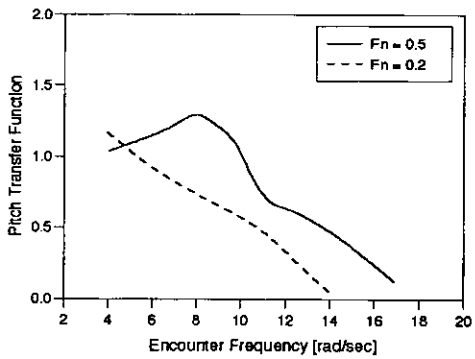

Figure 81b: Pitch

Figure 81: Model 4b $S/L = 0.2$, Effect of F_n on Heave and Pitch

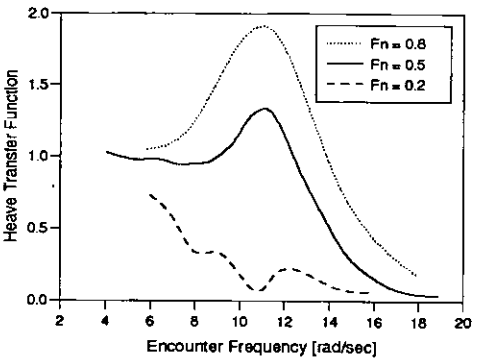

Figure 82a: Heave

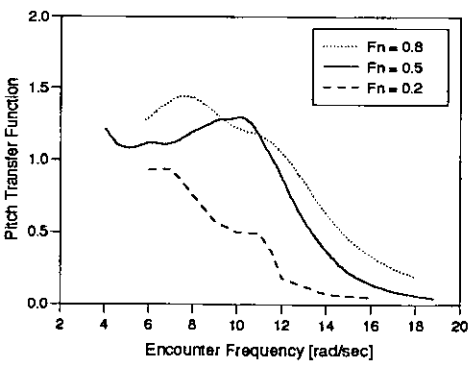

Figure 82b: Pitch

Figure 82: Model 4b $S/L = 0.4$, Effect of F_n on Heave and Pitch

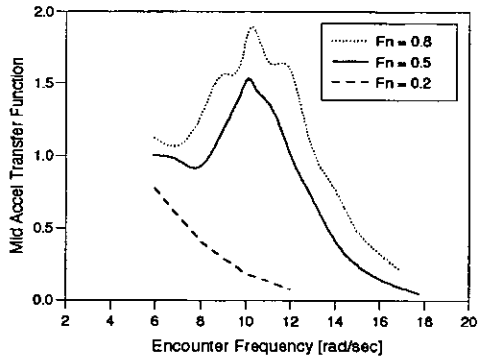

Figure 83a: Mid. Accel.

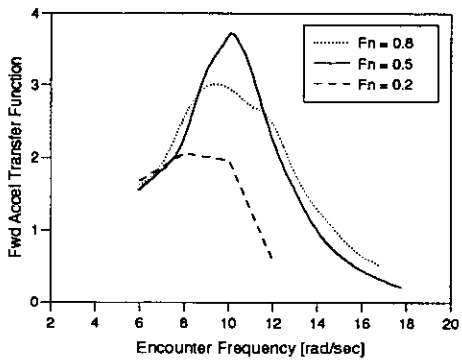

Figure 83b: Fwd. Accel.

Figure 83: Model 4b Monohull, Effect of F_n on Accelerations

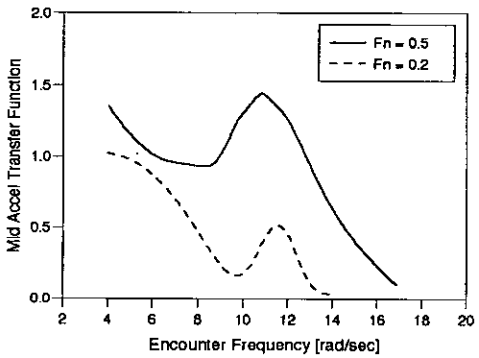

Figure 84a: Mid. Accel.

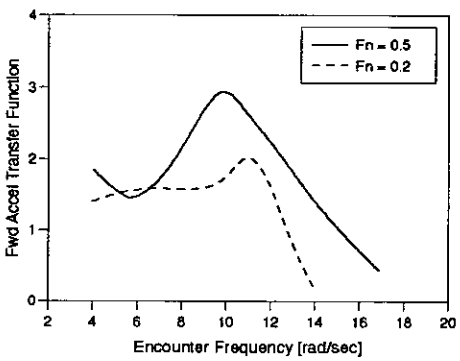

Figure 84b: Fwd. Accel.

Figure 84: Model 4b $S/L = 0.2$, Effect of F_n on Accelerations

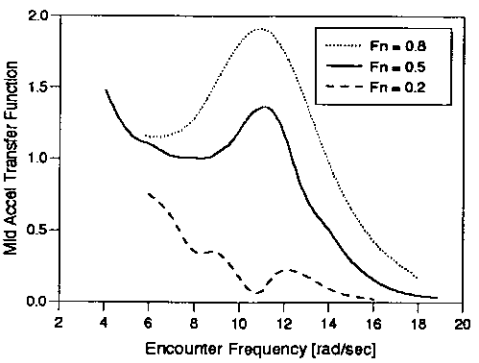

Figure 85a: Mid. Accel.

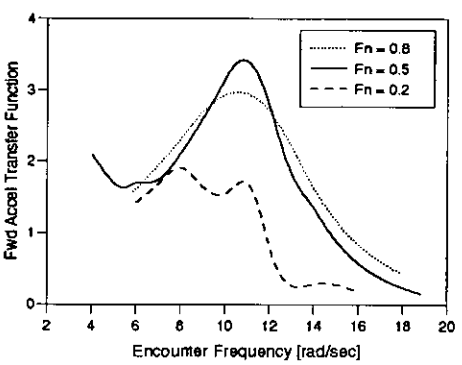

Figure 85b: Fwd. Accel.

Figure 85: Model 4b $S/L = 0.4$, Effect of F_n on Accelerations

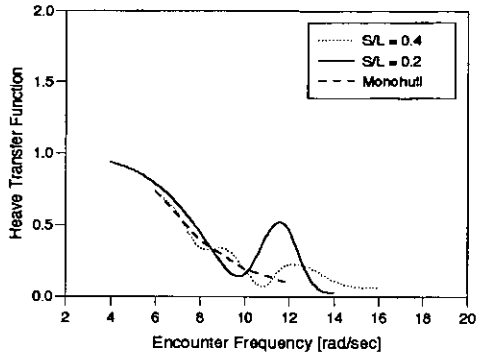

Figure 86a: Heave

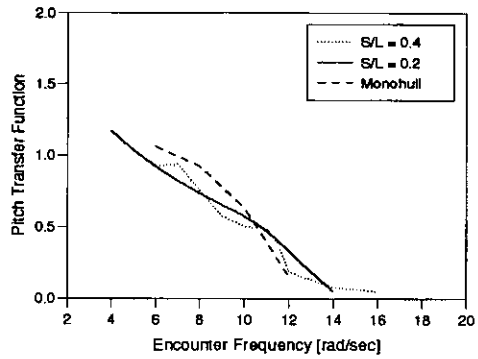

Figure 86b: Pitch

Figure 86: Model 4b $F_n = 0.2$, Effect of S/L on Heave and Pitch

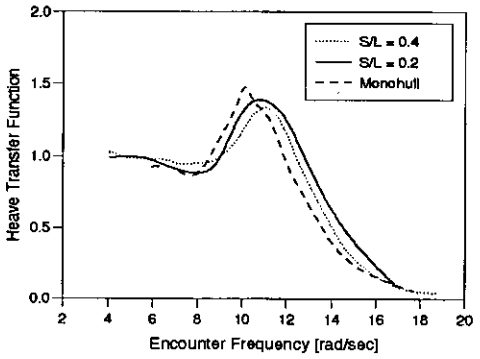

Figure 87a: Heave

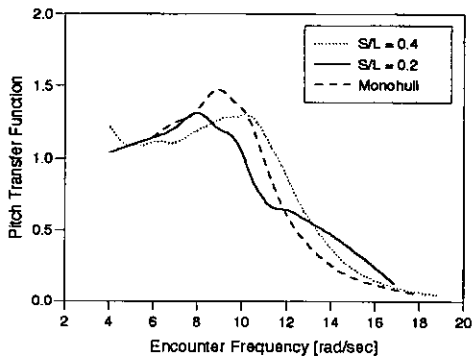

Figure 87b: Pitch

Figure 87: Model 4b $F_n = 0.53$, Effect of S/L on Heave and Pitch

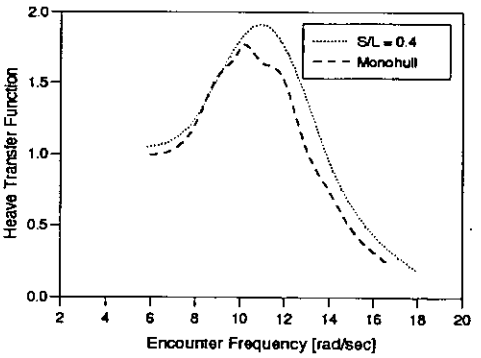

Figure 88a: Heave

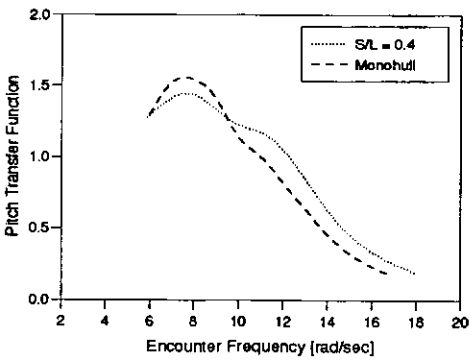

Figure 88b: Pitch

Figure 88: Model 4b $F_n = 0.8$, Effect of S/L on Heave and Pitch

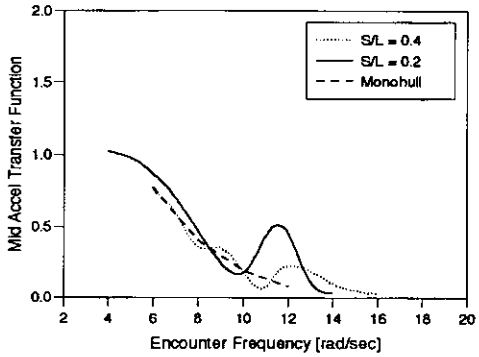

Figure 89a: Mid. Accel.

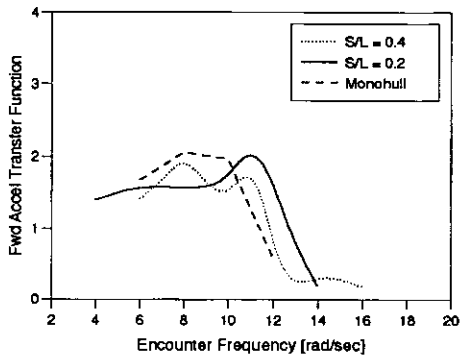

Figure 89b: Fwd. Accel.

Figure 89: Model 4b $F_n = 0.2$, Effect of S/L on Accelerations

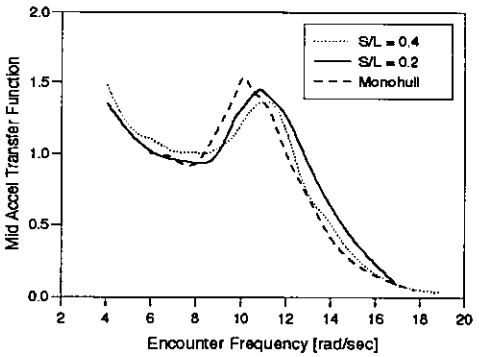

Figure 90a: Mid. Accel.

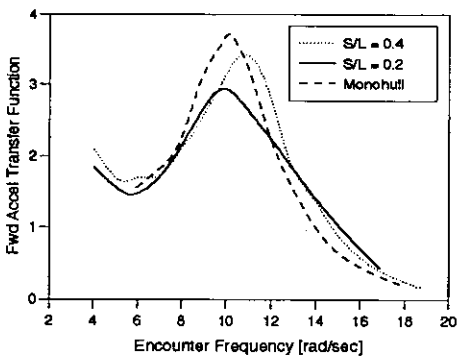

Figure 90b: Fwd. Accel.

Figure 90: Model 4b $F_n = 0.53$, Effect of S/L on Accelerations

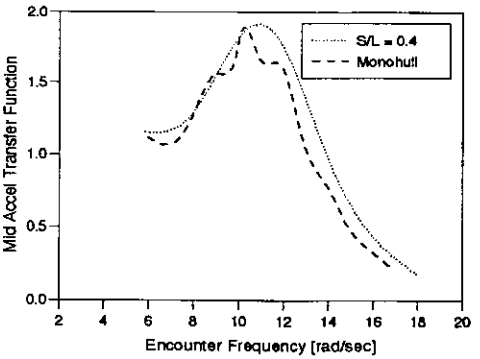

Figure 91a: Mid. Accel.

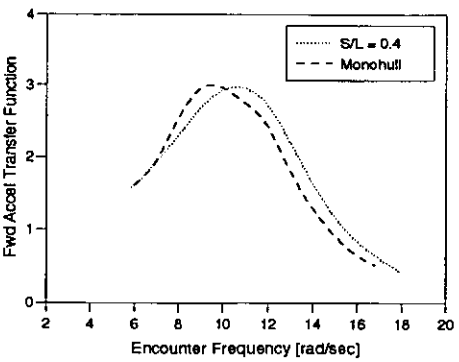

Figure 91b: Fwd. Accel.

Figure 91: Model 4b $F_n = 0.8$, Effect of S/L on Accelerations

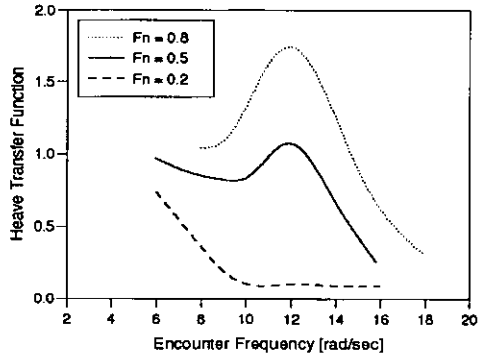

Figure 92a: Heave

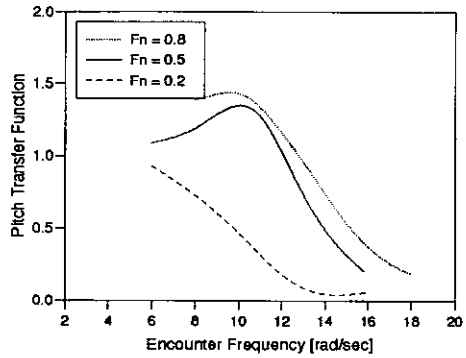

Figure 92b: Pitch

Figure 92: Model 5b Monohull, Effect of F_n on Heave and Pitch

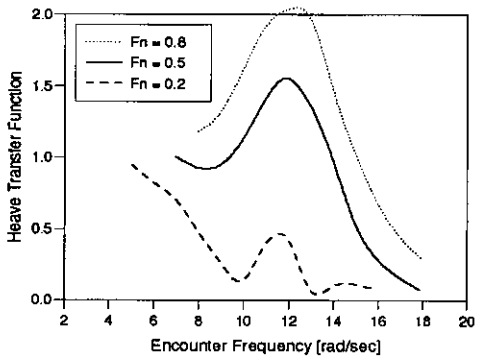

Figure 93a: Heave

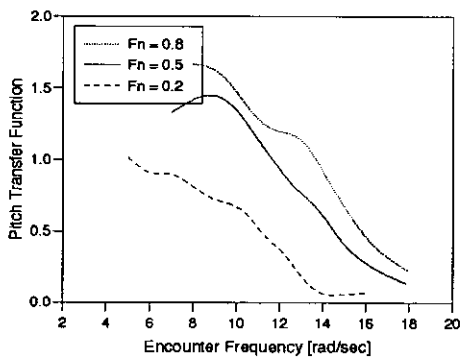

Figure 93b: Pitch

Figure 93: Model 5b $S/L = 0.2$, Effect of F_n on Heave and Pitch

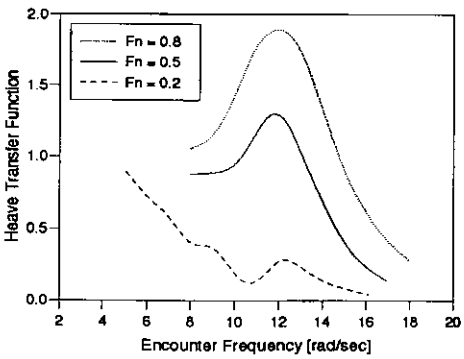

Figure 94a: Heave

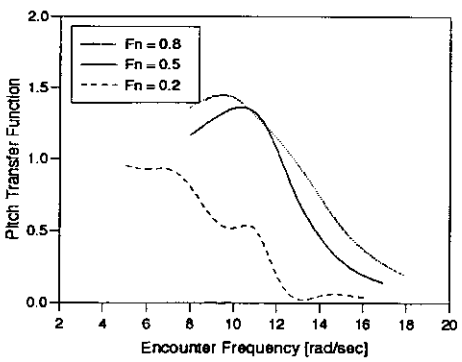

Figure 94b: Pitch

Figure 94: Model 5b $S/L = 0.4$, Effect of F_n on Heave and Pitch

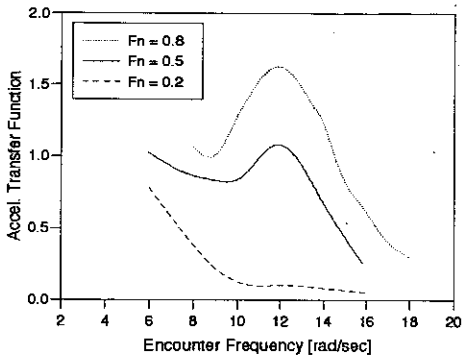

Figure 95a: Mid. Accel.

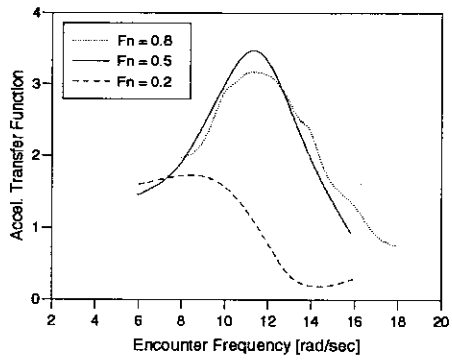

Figure 95b: Fwd. Accel.

Figure 95: Model 5b Monohull, Effect of F_n on Accelerations

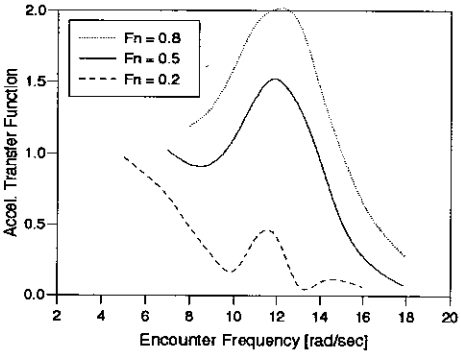

Figure 96a: Mid. Accel.

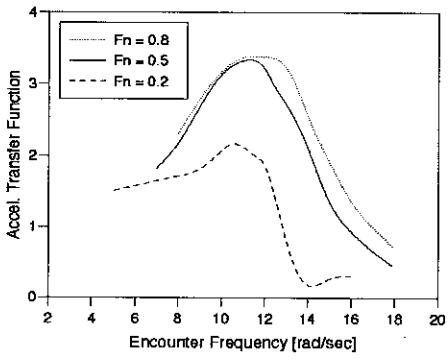

Figure 96b: Fwd. Accel.

Figure 96: Model 5b $S/L = 0.2$, Effect of F_n on Accelerations

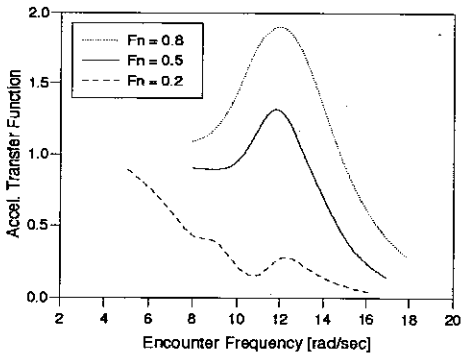

Figure 97a: Mid. Accel.

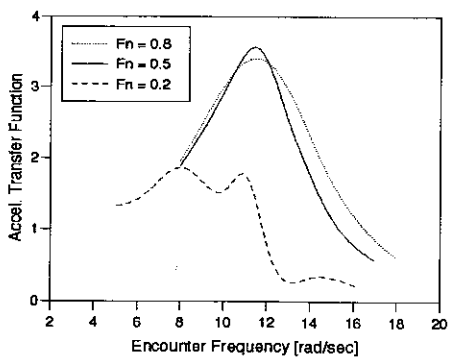

Figure 97b: Fwd. Accel.

Figure 97: Model 5b $S/L = 0.4$, Effect of F_n on Accelerations

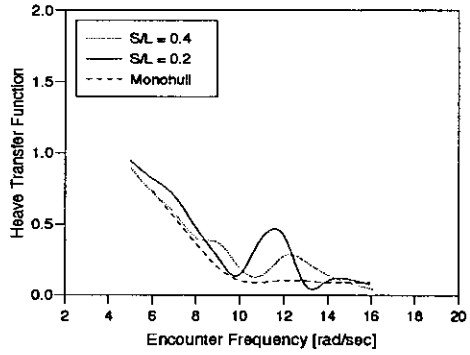

Figure 98a: Heave

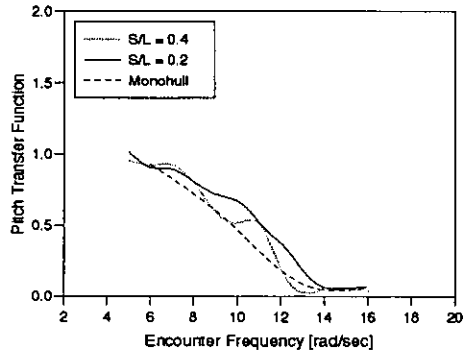

Figure 98b: Pitch

Figure 98: Model 5b $F_n = 0.2$, Effect of S/L on Heave and Pitch

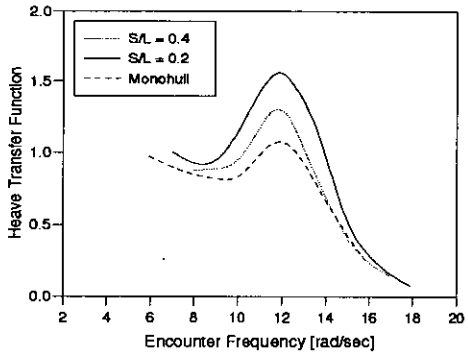

Figure 99a: Heave

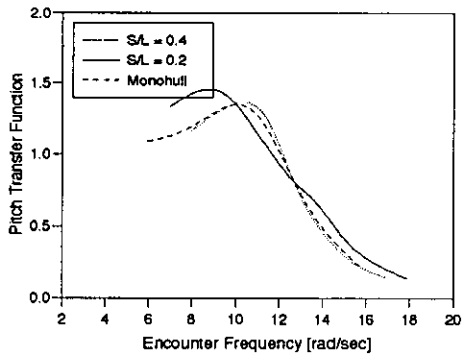

Figure 99b: Pitch

Figure 99: Model 5b $F_n = 0.53$, Effect of S/L on Heave and Pitch

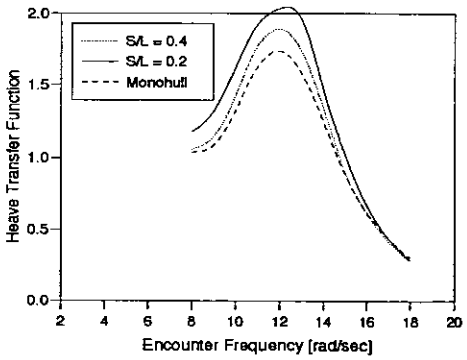

Figure 100a: Heave

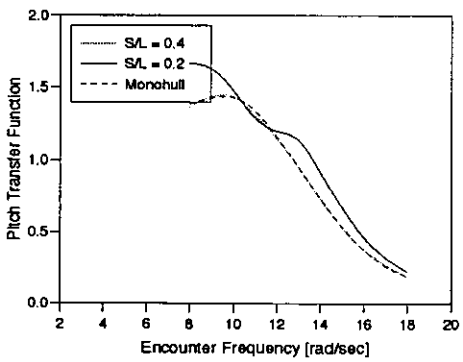

Figure 100b: Pitch

Figure 100: Model 5b $F_n = 0.8$, Effect of S/L on Heave and Pitch

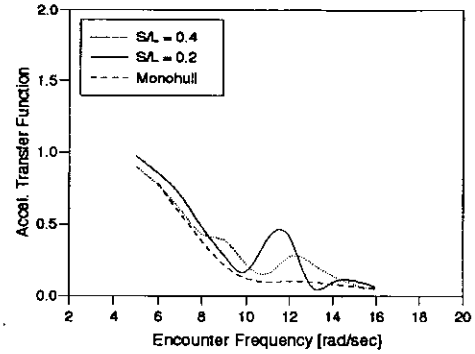

Figure 101a: Mid. Accel.

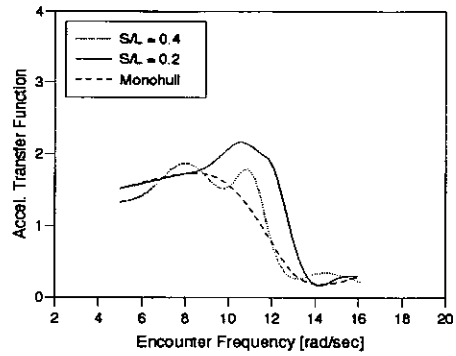

Figure 101b: Fwd. Accel.

Figure 101: Model 5b $F_n = 0.2$, Effect of S/L on Accelerations

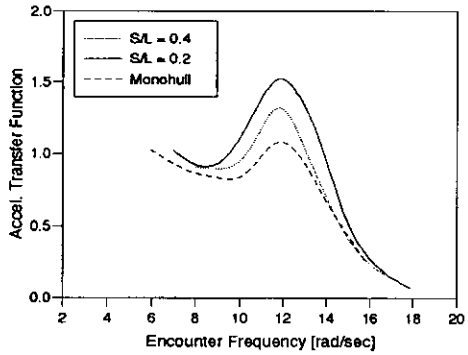

Figure 102a: Mid. Accel.

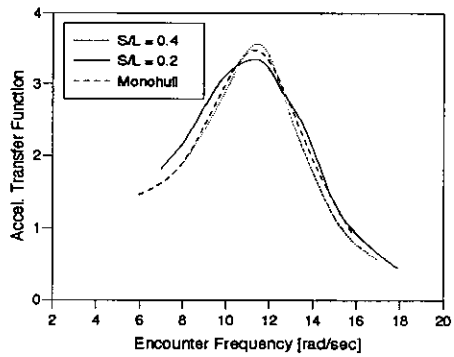

Figure 102b: Fwd. Accel.

Figure 102: Model 5b $F_n = 0.53$, Effect of S/L on Accelerations

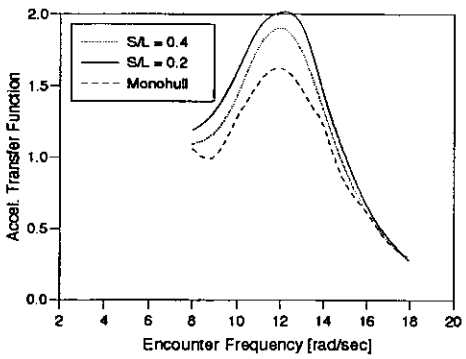

Figure 103a: Mid. Accel.

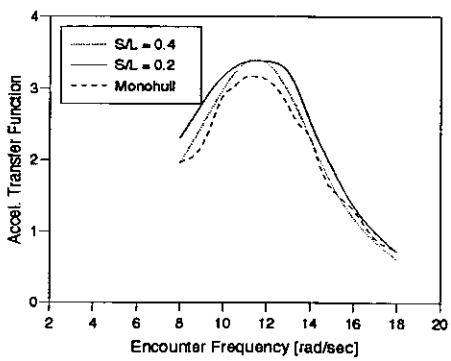

Figure 103b: Fwd. Accel.

Figure 103: Model 5b $F_n = 0.8$, Effect of S/L on Accelerations

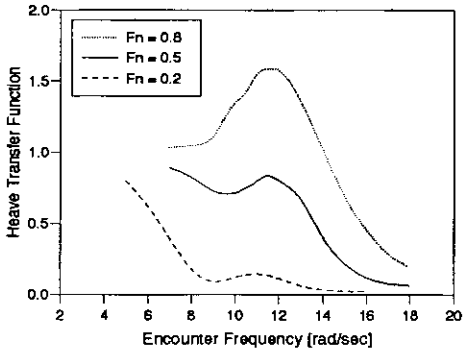

Figure 104a: Heave

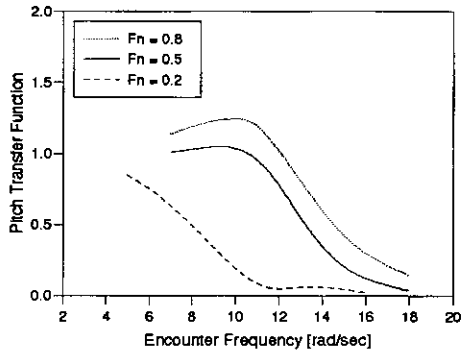

Figure 104b: Pitch

Figure 104: Model 6b Monohull, Effect of F_n on Heave and Pitch

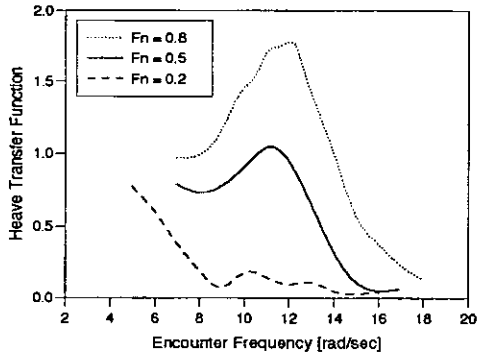

Figure 105a: Heave

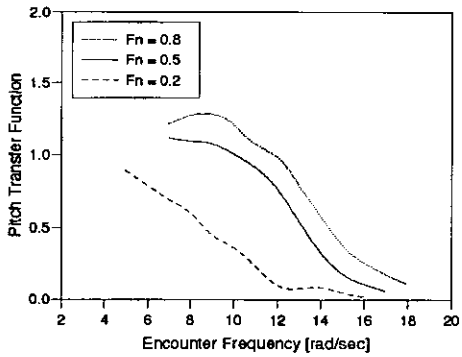

Figure 105b: Pitch

Figure 105: Model 6b $S/L = 0.2$, Effect of F_n on Heave and Pitch

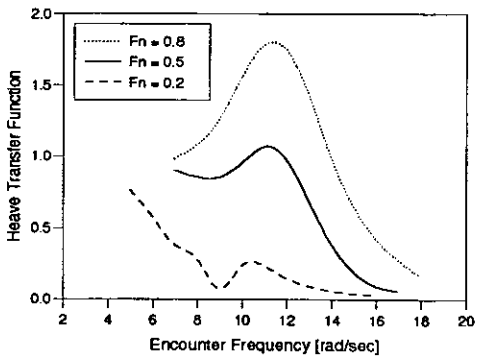

Figure 106a: Heave

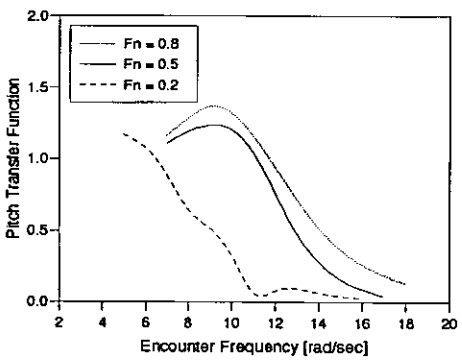

Figure 106b: Pitch

Figure 106: Model 6b $S/L = 0.4$, Effect of F_n on Heave and Pitch

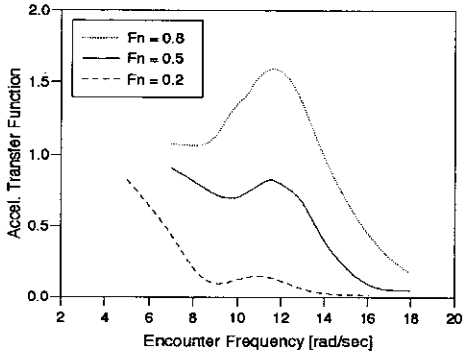

Figure 107a: Mid. Accel.

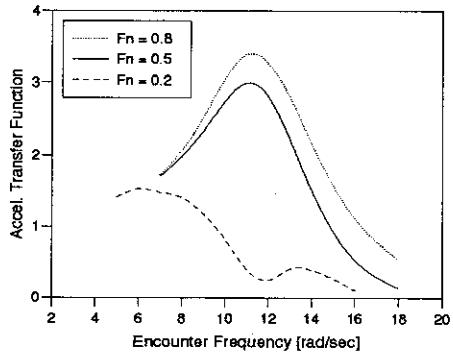

Figure 107b: Fwd. Accel.

Figure 107: Model 6b Monohull, Effect of F_n on Accelerations

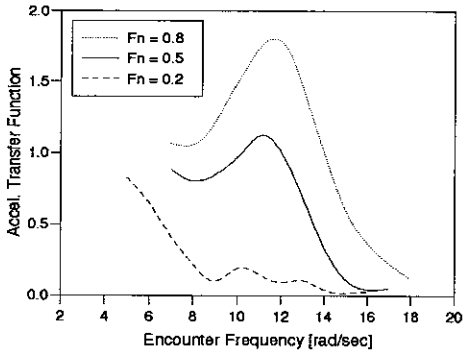

Figure 108a: Mid. Accel.

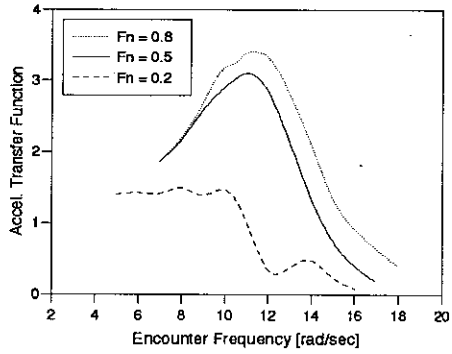

Figure 108b: Fwd. Accel.

Figure 108: Model 6b $S/L = 0.2$, Effect of F_n on Accelerations

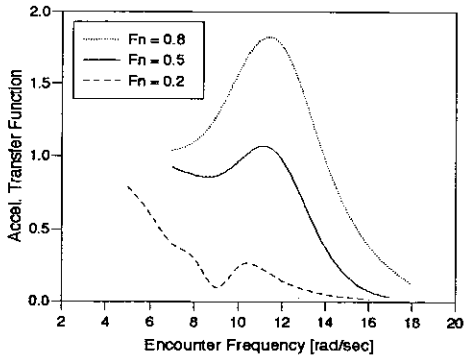

Figure 109a: Mid. Accel.

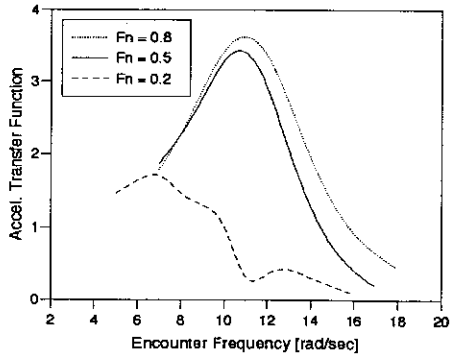

Figure 109b: Fwd. Accel.

Figure 109: Model 6b $S/L = 0.4$, Effect of F_n on Accelerations

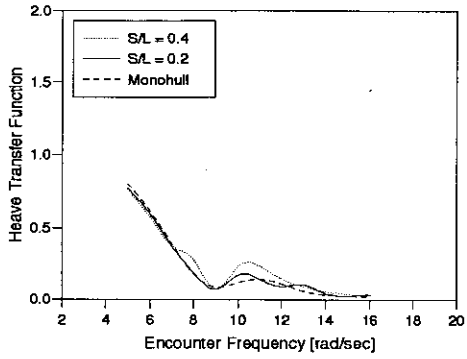

Figure 110a: Heave

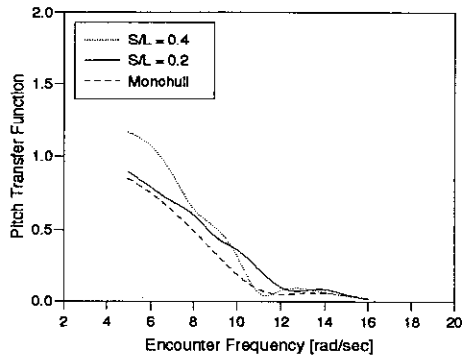

Figure 110b: Pitch

Figure 110: Model 6b $F_n = 0.2$, Effect of S/L on Heave and Pitch

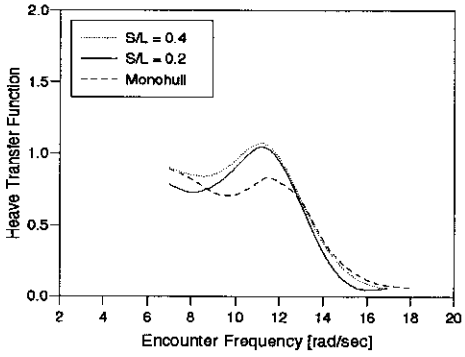

Figure 111a: Heave

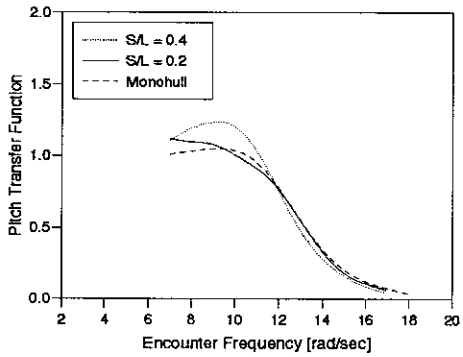

Figure 111b: Pitch

Figure 111: Model 6b $F_n = 0.53$, Effect of S/L on Heave and Pitch

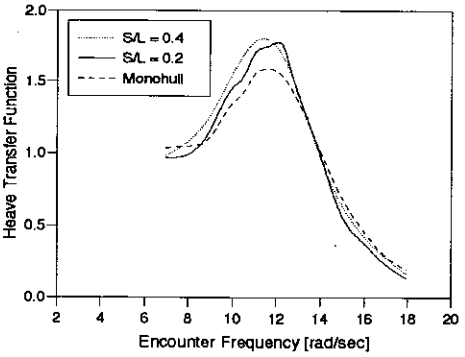

Figure 112a: Heave

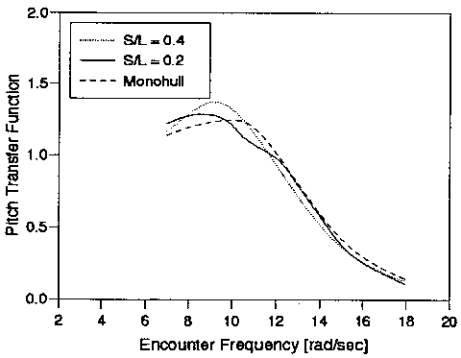

Figure 112b: Pitch

Figure 112: Model 6b $F_n = 0.8$, Effect of S/L on Heave and Pitch

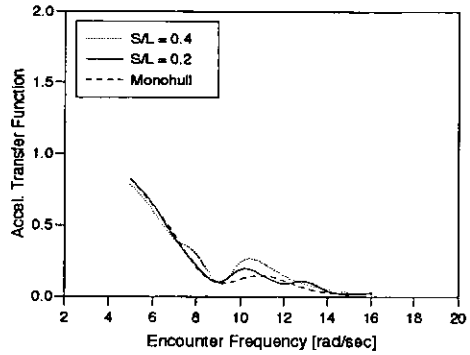

Figure 113a: Mid. Accel.

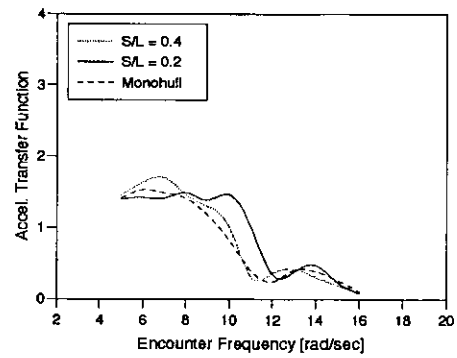

Figure 113b: Fwd. Accel.

Figure 113: Model 6b $F_n = 0.2$, Effect of S/L on Accelerations

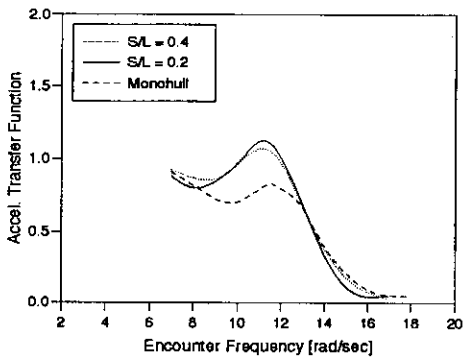

Figure 114a: Mid. Accel.

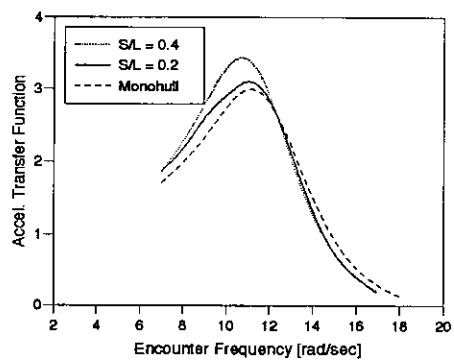

Figure 114b: Fwd. Accel.

Figure 114: Model 6b $F_n = 0.53$, Effect of S/L on Accelerations

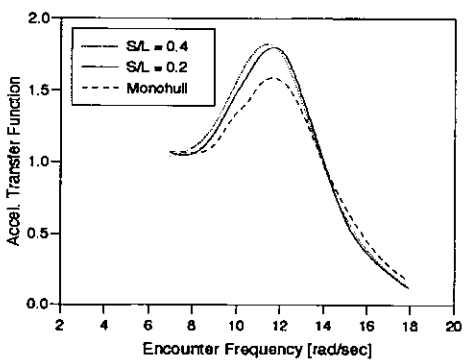

Figure 115a: Mid. Accel.

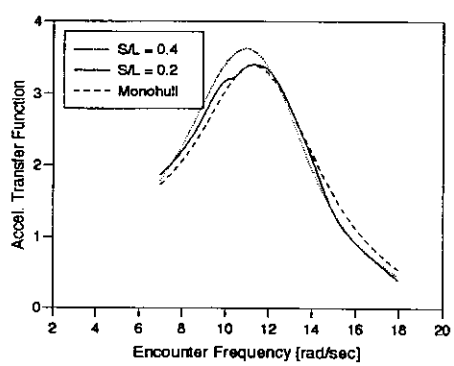

Figure 115b: Fwd. Accel.

Figure 115: Model 6b $F_n = 0.8$, Effect of S/L on Accelerations

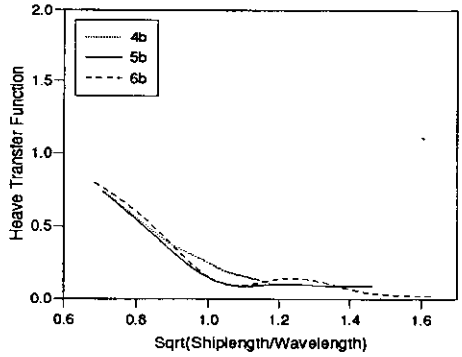

Figure 116a: Heave

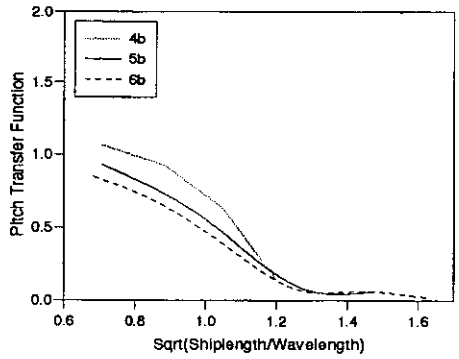

Figure 116b: Pitch

Figure 116: Monohull, $F_n = 0.2$, Effect of $L/\nabla^{\frac{1}{3}}$ on Heave and Pitch

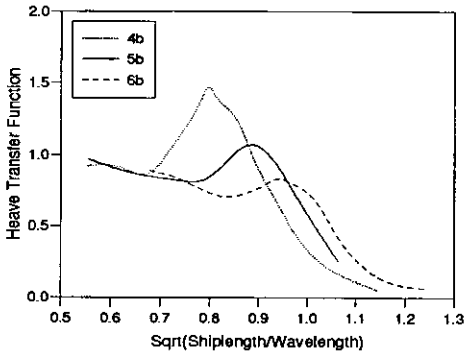

Figure 117a: Heave

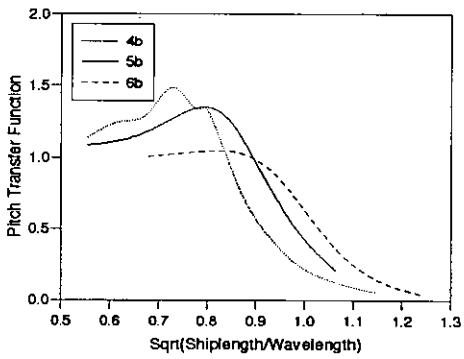

Figure 117b: Pitch

Figure 117: Monohull, $F_n = 0.53$, Effect of $L/\nabla^{\frac{1}{3}}$ on Heave and Pitch

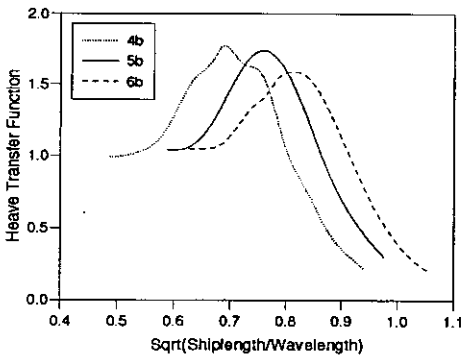

Figure 118a: Heave

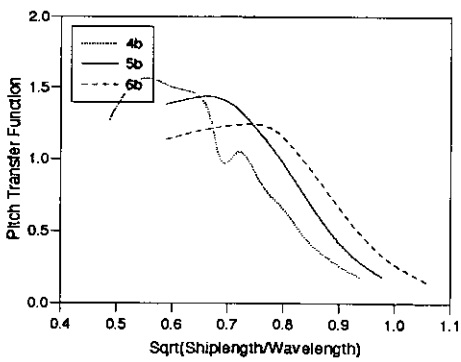

Figure 118b: Pitch

Figure 118: Monohull, $F_n = 0.8$, Effect of $L/\nabla^{\frac{1}{3}}$ on Heave and Pitch

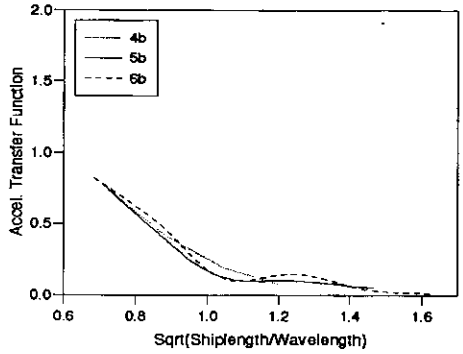

Figure 119a: Mid. Accel.

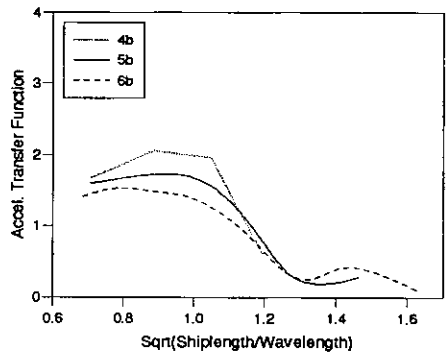

Figure 119b: Fwd. Accel.

Figure 119: Monohull, $F_n = 0.2$, Effect of $L/\nabla^{\frac{1}{3}}$ on Accelerations

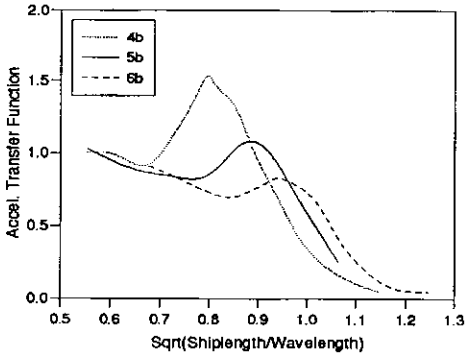

Figure 120a: Mid. Accel.

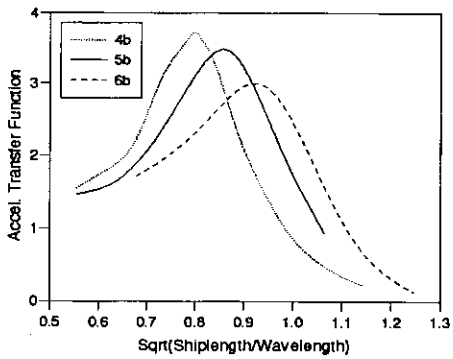

Figure 120b: Fwd. Accel.

Figure 120: Monohull, $F_n = 0.53$, Effect of $L/\nabla^{\frac{1}{3}}$ on Accelerations

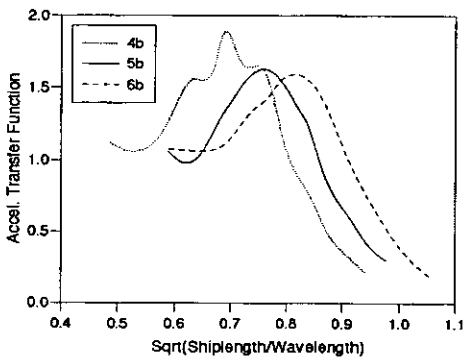

Figure 121a: Mid. Accel.

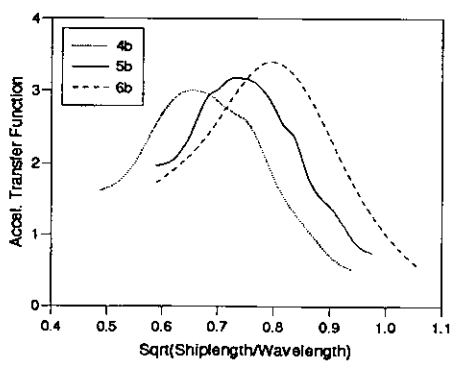

Figure 121b: Fwd. Accel.

Figure 121: Monohull, $F_n = 0.8$, Effect of $L/\nabla^{\frac{1}{3}}$ on Accelerations

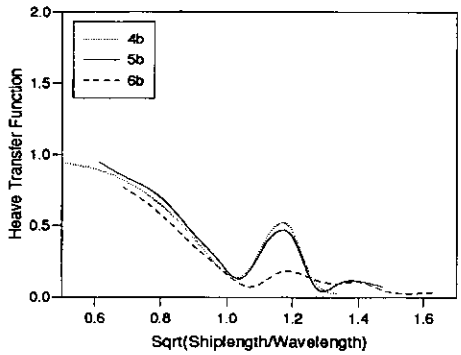

Figure 122a: Heave

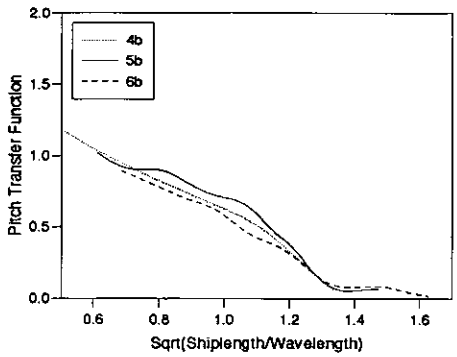

Figure 122b: Pitch

Figure 122: $S/L = 0.2$, $F_n = 0.2$, Effect of $L/\nabla^{\frac{1}{3}}$ on Heave and Pitch

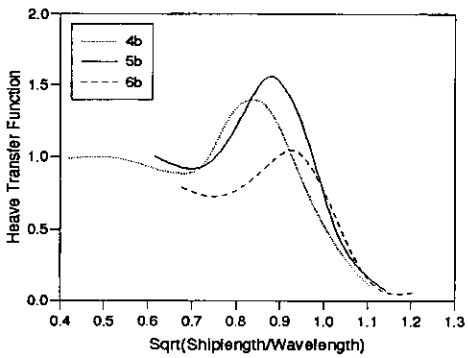

Figure 123a: Heave

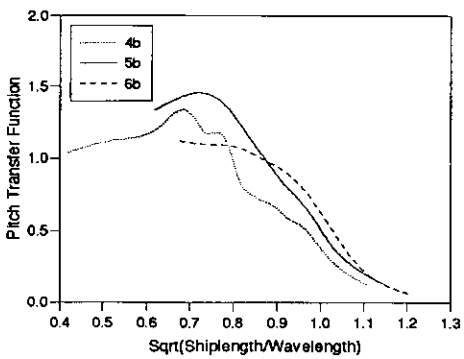

Figure 123b: Pitch

Figure 123: $S/L = 0.2$, $F_n = 0.53$, Effect of $L/\nabla^{\frac{1}{3}}$ on Heave and Pitch

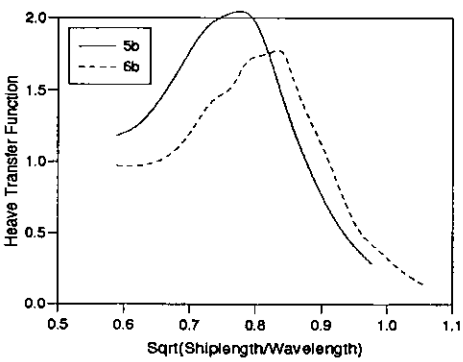

Figure 124a: Heave

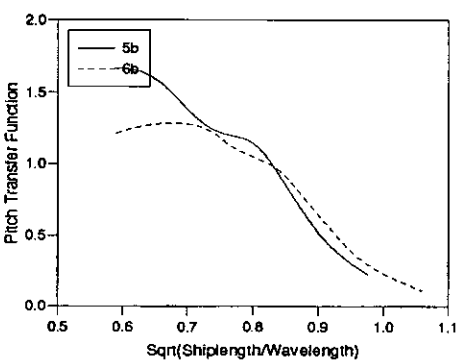

Figure 124b: Pitch

Figure 124: $S/L = 0.2$, $F_n = 0.8$, Effect of $L/\nabla^{\frac{1}{3}}$ on Heave and Pitch

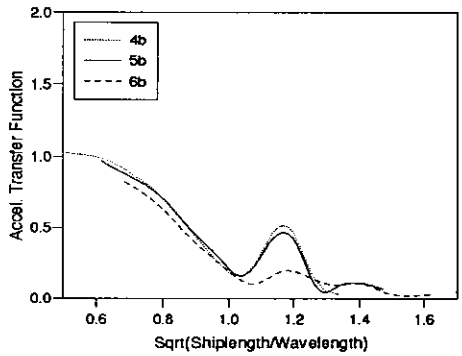

Figure 125a: Mid. Accel.

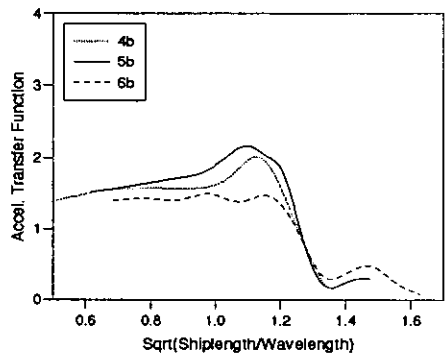

Figure 125b: Fwd. Accel.

Figure 125: $S/L = 0.2$, $F_n = 0.2$, Effect of $L/\nabla^{\frac{1}{3}}$ on Accelerations

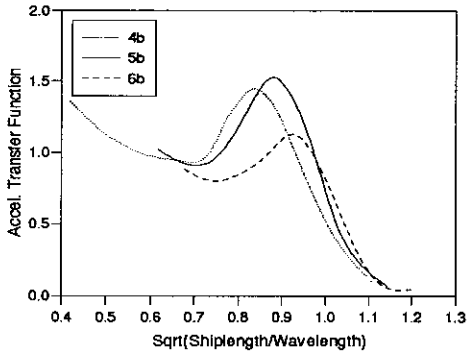

Figure 126a: Mid. Accel.

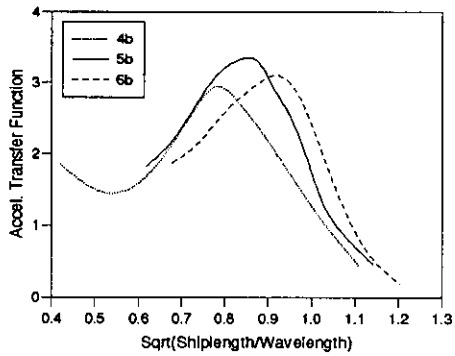

Figure 126b: Fwd. Accel.

Figure 126: $S/L = 0.2$, $F_n = 0.53$, Effect of $L/\nabla^{\frac{1}{3}}$ on Accelerations

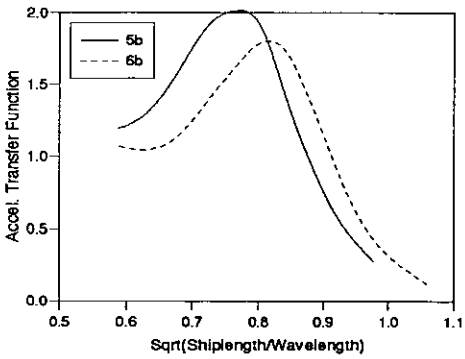

Figure 127a: Mid. Accel.

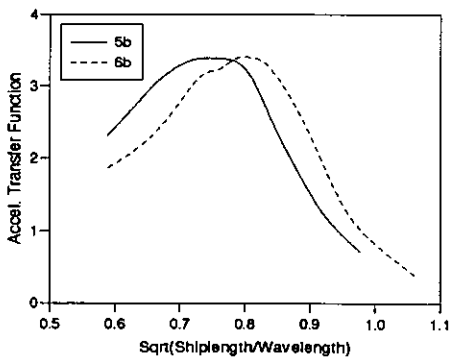

Figure 127b: Fwd. Accel.

Figure 127: $S/L = 0.2$, $F_n = 0.8$, Effect of $L/\nabla^{\frac{1}{3}}$ on Accelerations

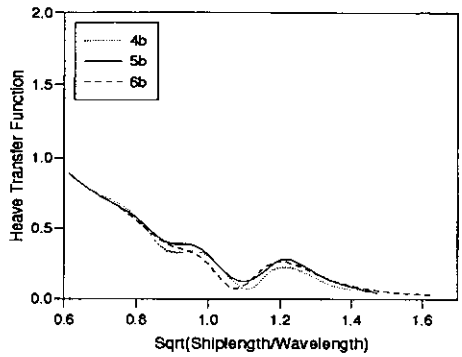

Figure 128a: Heave

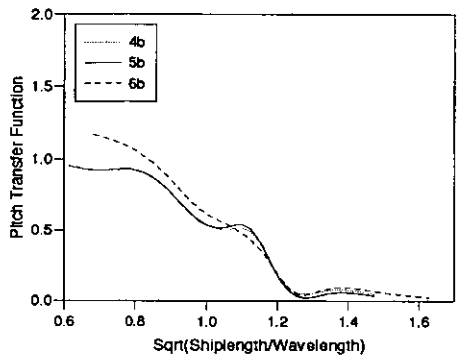

Figure 128b: Pitch

Figure 128: $S/L = 0.4$, $F_n = 0.2$, Effect of $L/\nabla^{\frac{1}{3}}$ on Heave and Pitch

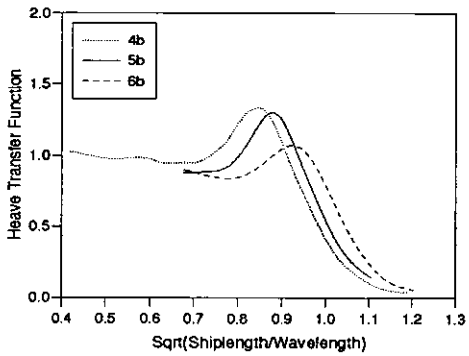

Figure 129a: Heave

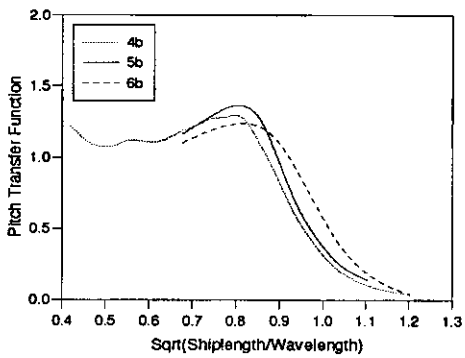

Figure 129b: Pitch

Figure 129: $S/L = 0.4$, $F_n = 0.53$, Effect of $L/\nabla^{\frac{1}{3}}$ on Heave and Pitch

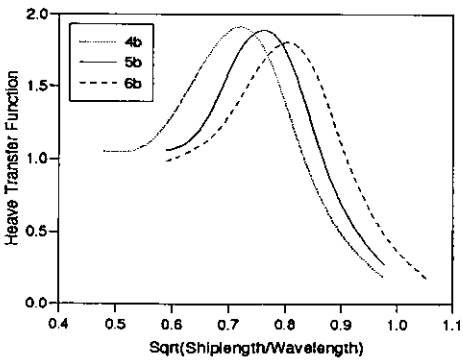

Figure 130a: Heave

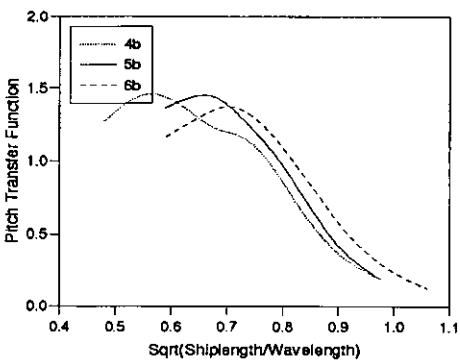

Figure 130b: Pitch

Figure 130: $S/L = 0.4$, $F_n = 0.8$, Effect of $L/\nabla^{\frac{1}{3}}$ on Heave and Pitch

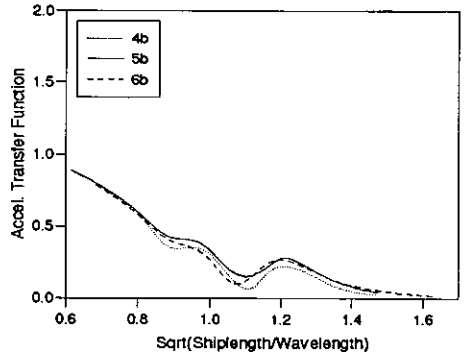

Figure 131a: Mid. Accel.

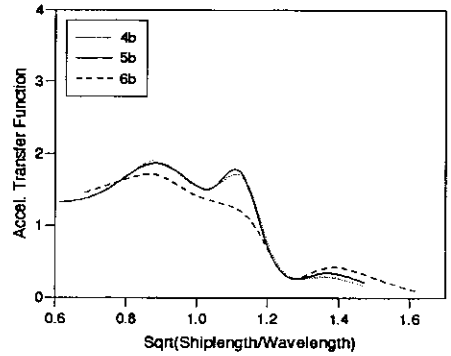

Figure 131b: Fwd. Accel.

Figure 131: $S/L = 0.4$, $F_n = 0.2$, Effect of $L/\nabla^{\frac{1}{3}}$ on Accelerations

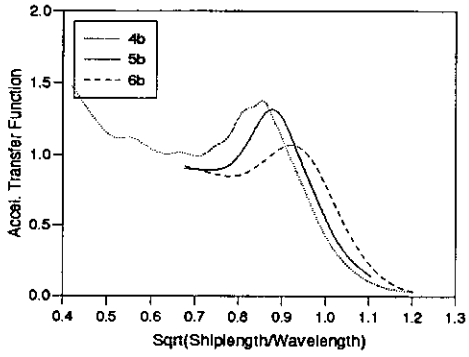

Figure 132a: Mid. Accel.

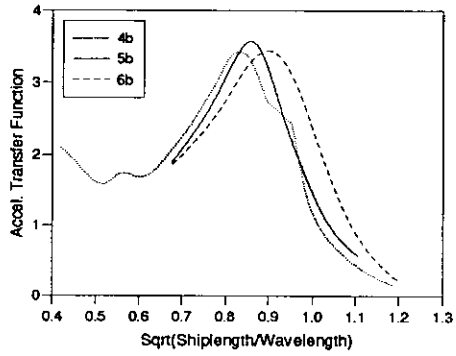

Figure 132b: Fwd. Accel.

Figure 132: $S/L = 0.4$, $F_n = 0.53$, Effect of $L/\nabla^{\frac{1}{3}}$ on Accelerations

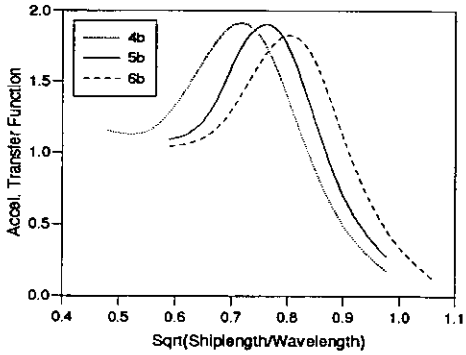

Figure 133a: Mid. Accel.

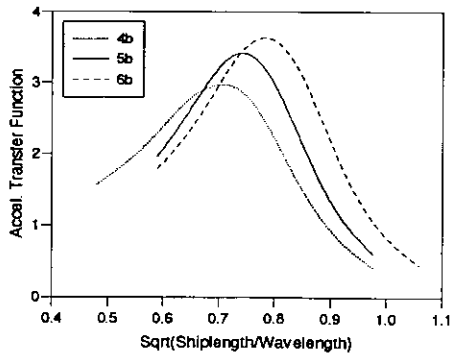

Figure 133b: Fwd. Accel.

Figure 133: $S/L = 0.4$, $F_n = 0.8$, Effect of $L/\nabla^{\frac{1}{3}}$ on Accelerations

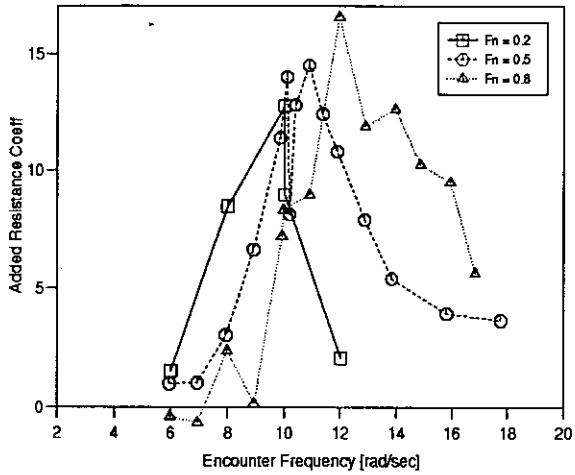

Figure 134: Model 4b Monohull, Added Resistance

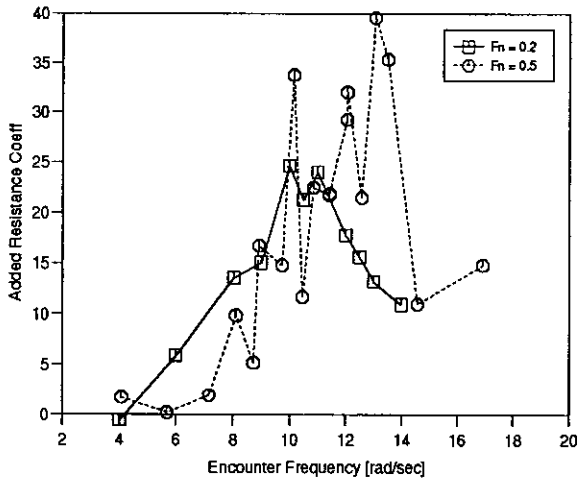

Figure 135: Model 4b $S/L = 0.2$, Added Resistance

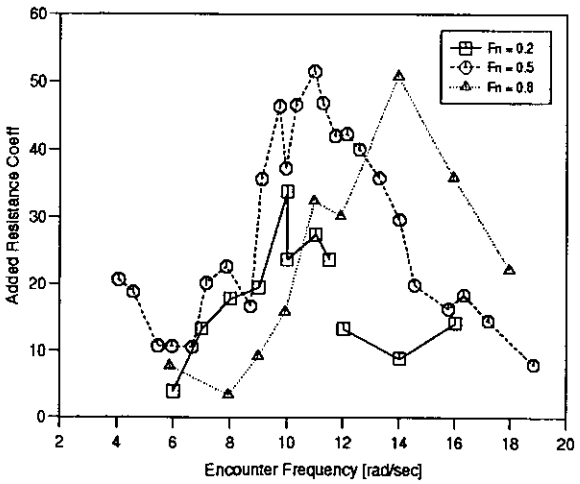

Figure 136: Model 4b $S/L = 0.4$, Added Resistance

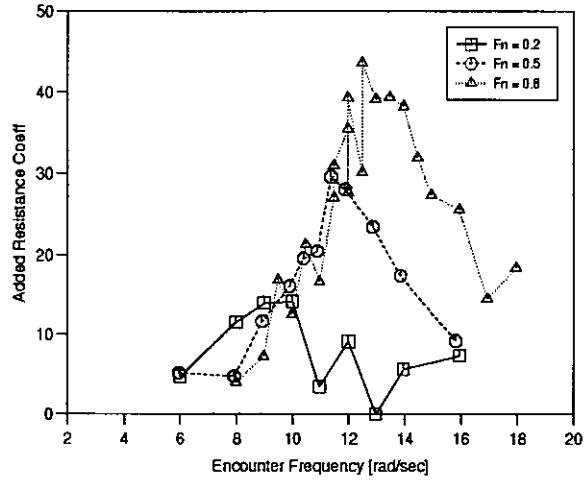

Figure 137: Model 5b Monohull, Added Resistance

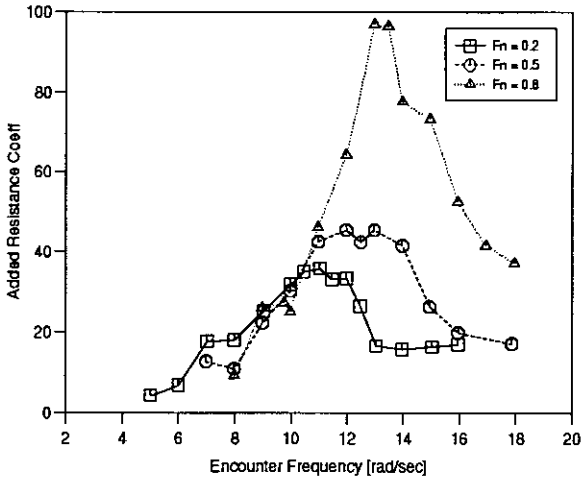

Figure 138: Model 5b $S/L = 0.2$, Added Resistance

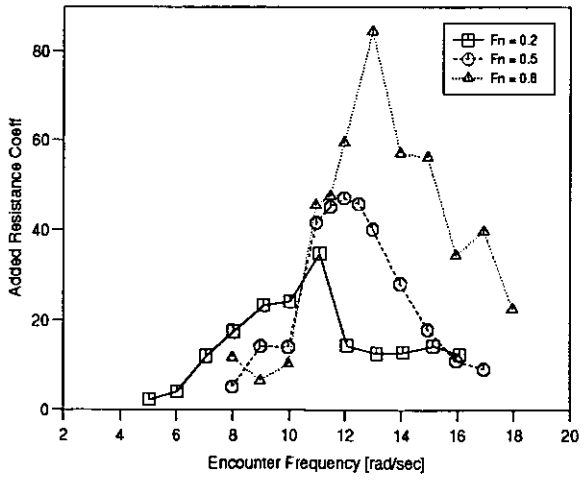

Figure 139: Model 5b $S/L = 0.4$, Added Resistance

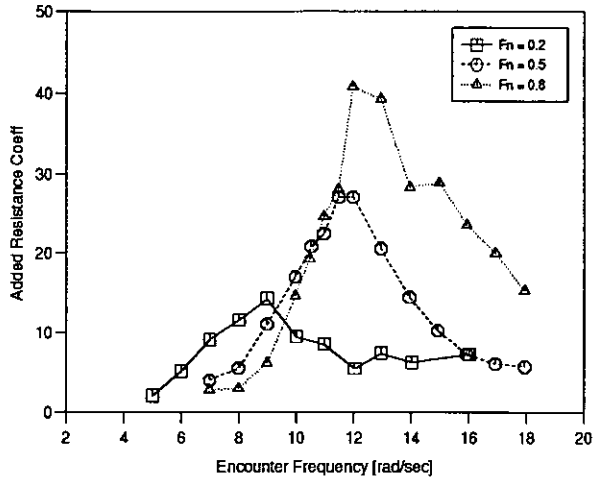

Figure 140: Model 6b Monohull, Added Resistance

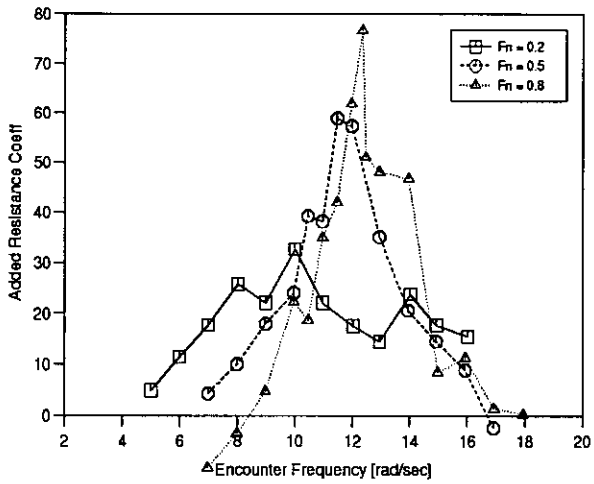

Figure 141: Model 6b $S/L = 0.2$, Added Resistance

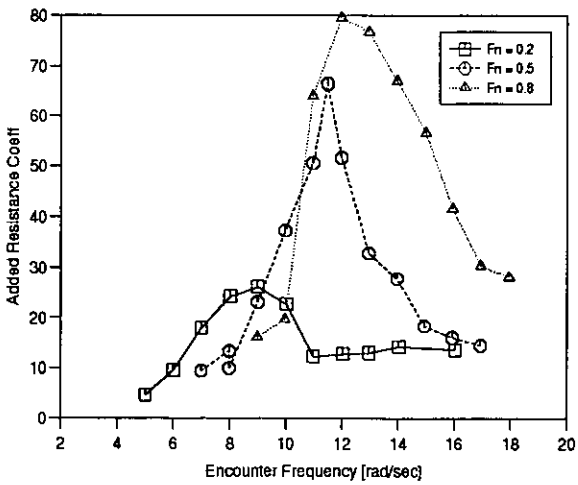

Figure 142: Model 6b $S/L = 0.4$, Added Resistance

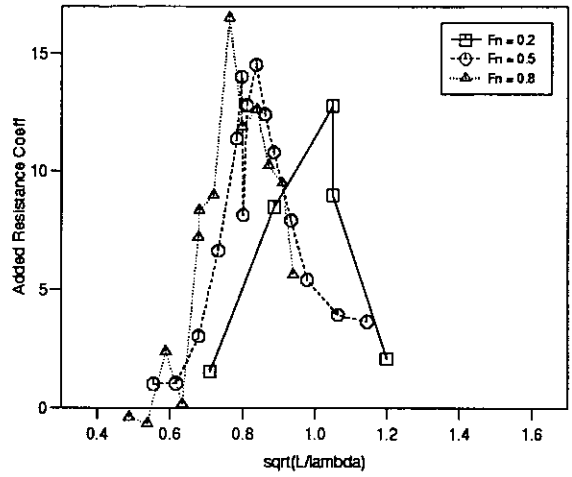

Figure 143: Model 4b Monohull, Added Resistance (vs sqrt(L/lambda))

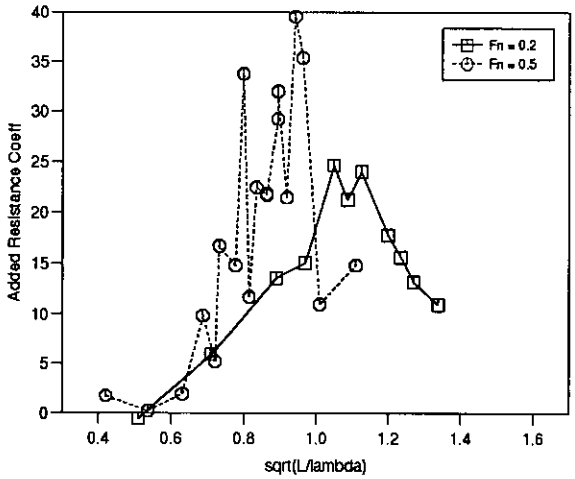

Figure 144: Model 4b $S/L = 0.2$, Added Resistance (vs sqrt(L/lambda))

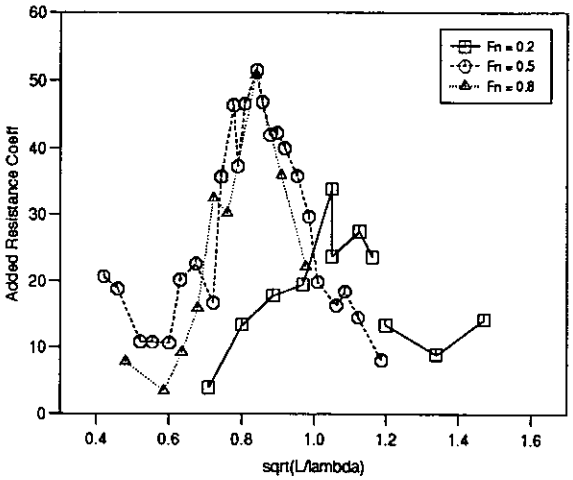

Figure 145: Model 4b $S/L = 0.4$, Added Resistance (vs sqrt(L/lambda))

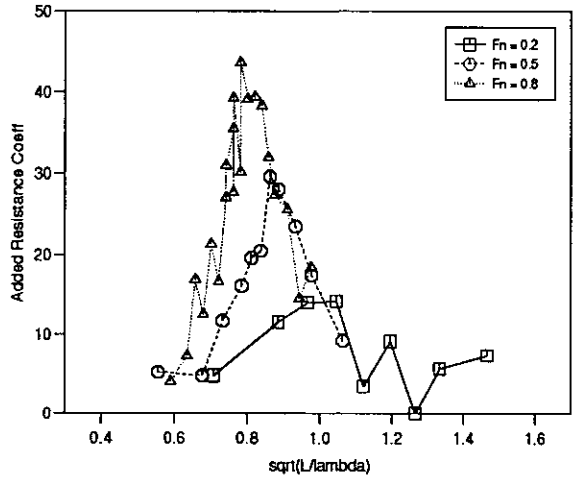

Figure 146: Model 5b Monohull, Added Resistance (vs sqrt(L/lambda))

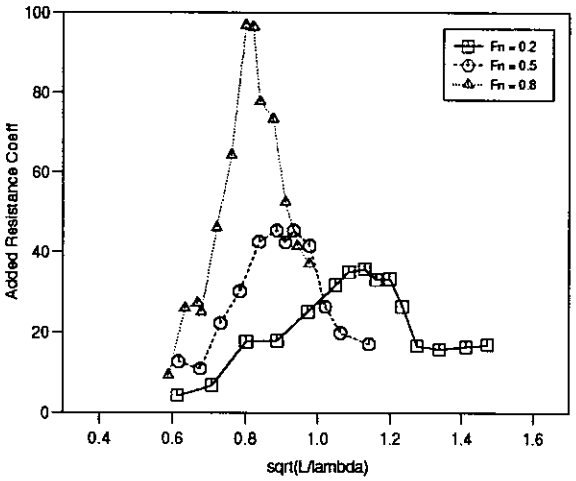

Figure 147: Model 5b $S/L = 0.2$, Added Resistance (vs sqrt(L/lambda))

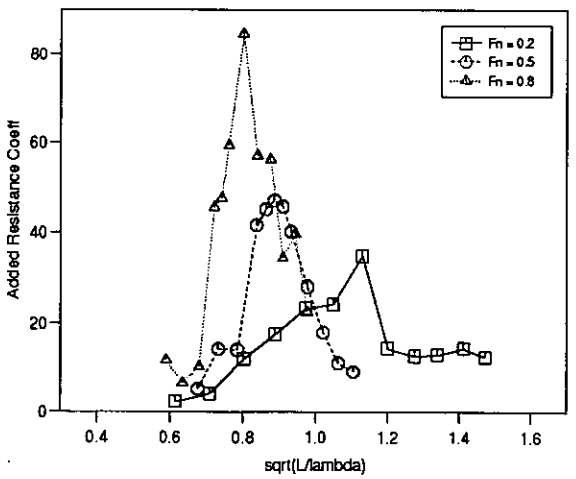

Figure 148: Model 5b $S/L = 0.4$, Added Resistance (vs sqrt(L/lambda))

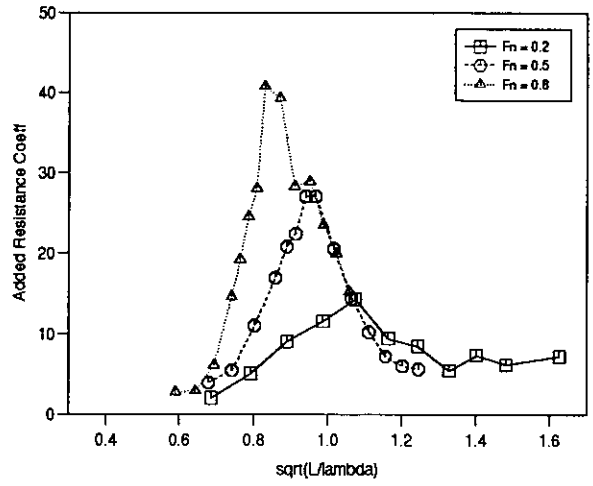

Figure 149: Model 6b Monohull, Added Resistance (vs sqrt(L/lambda))

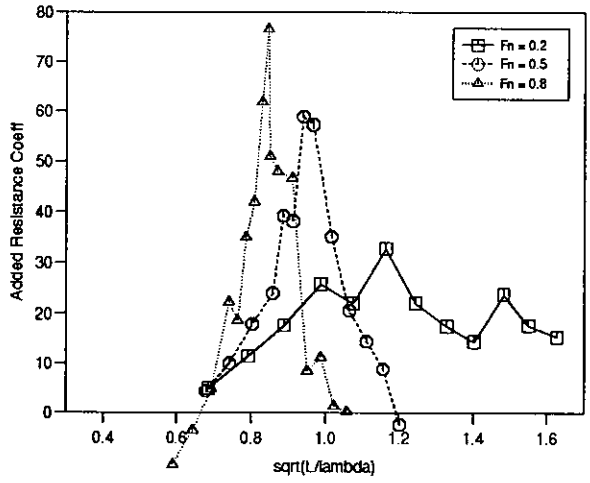

Figure 150: Model 6b $S/L = 0.2$, Added Resistance (vs sqrt(L/lambda))

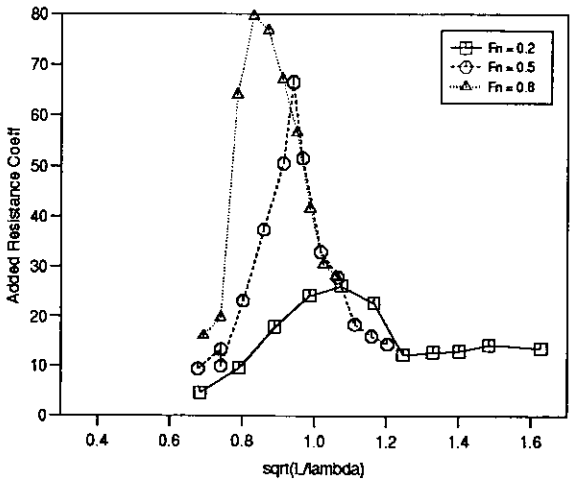

Figure 151: Model 6b $S/L = 0.4$, Added Resistance (vs sqrt(L/lambda))

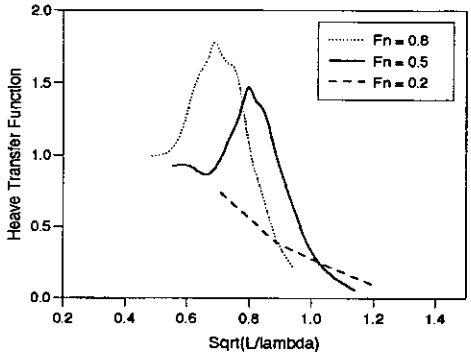

Figure 152a: 4b monohull

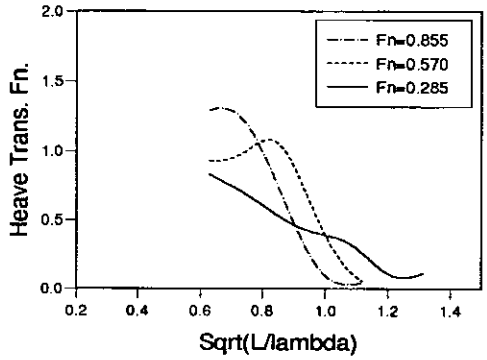

Figure 152b: Blok and Beukelman

Figure 152: Comparison of Heave

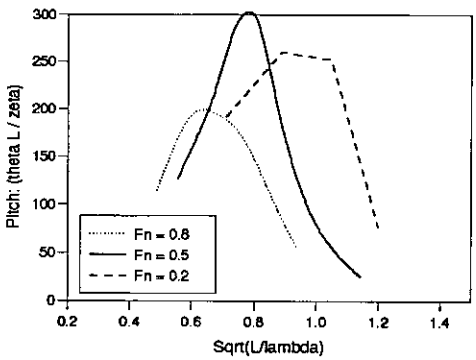

Figure 152a: 4b monohull

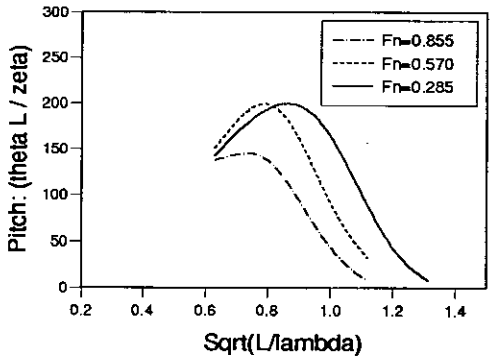

Figure 152b: Blok and Beukelman

Figure 153: Comparison of Pitch

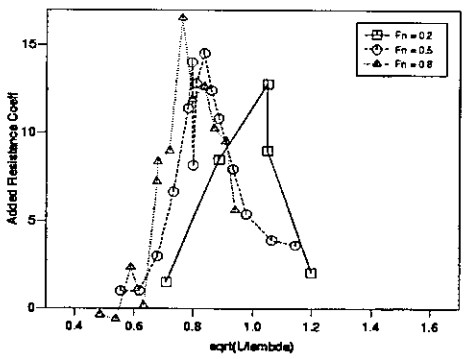

Figure 152a: 4b monohull

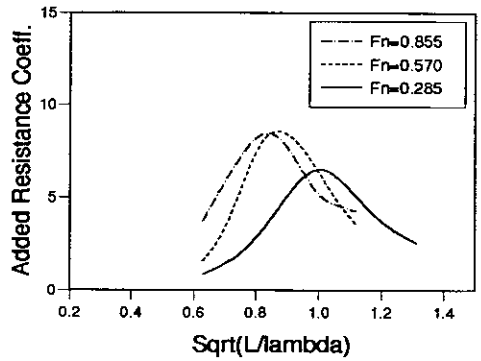

Figure 152b: Blok and Beukelman

Figure 154: Comparison of Added Resistance